WAVE PROPAGATION IN ELASTIC BARS COUPLED

BY VISCOELASTIC ELEMENT

by

ARUN KUMAR KAPOOR

B. Tech. Indian Institute of Technology,
Kanpur, India, 1967

A THESIS SUBMITTED IN PARTIAL FULFILMENT OF
THE REQUIREMENTS FOR THE DEGREE OF
MASTER OF APPLIED SCIENCE

in the Department

of

Mechanical Engineering

We accept this thesis as conforming to the

required standard

THE UNIVERSITY OF BRITISH COLUMBIA

April, 1969

In presenting this thesis in partial ful· iment of the requirements for

an advanced degree at the University of British Columbia, I agree that

the Library shall make it freely available for reference and Study.

I further agree that permission for extensive copying of this thesis

for scholarly purposes may be granted by the Head of my Department or

by his representatives. It is understood that copying or publication

of this thesis for financial gain shall not be allowed without my

written permission.

(Arun Kumar Kapoor)

Department of   Mechanical Engineering

The University of British Columbia
Vancouver 8, Canada

Date   April 29 , 1969

ABSTRACT

The split Hopkinson pressure bar has been used to
study the acoustic isolation that can be achieved by inserting
a compliant element into the sound path in an elastic system,
and to study the dynamic response of the material comprising
the compliant element. The specimens were inserted between two
steel transducer bars. The incident stress pulse, of about 100
microsecond duration, was produced by striking the free end of
one of the transducer bars by a round-headed striker bar. The
incident pulse in the first bar and the transmitted pulse in
the second bar were sensed by strain gages and displayed on an
oscilloscope.

The comparison of computed Fourier transforms (within
the acoustic frequency range) of both the incident and transmitted
pulses showed that in general a greater reduction in transmission
of vibration across a specimen is achieved:

  i) by increasing the length of the specimen;

 ii) by using a material with a higher attenuation constant
     or higher viscous damping;

iii) by increasing the impedance mismatch between the spec-
     imen and the steel transducer bars.

Also, it was found that isolation is greater at high
frequencies than at low frequencies.

CORRIGENDA

Page	Line	Change
Abstract	13	audible not acoustic
List of Figures	12	Sine not since
Nomenclature	14	Inverse not Iniverse
1	6 up	specimens not specimen
2	9	audible not acoustic
5	1	(3.1.10) not (3.1.8)
5	4,6,7,13	c^* not $\bar{c}$ or c
5	11	$(i\omega t)$ not $(i\omega T)$
7	9 up	[12] not [6]
8	12	[13] not [6]
15	3	$-\lambda_1 h(t+\frac{x}{c_o})$ not $h(t+\frac{x}{c_o})$
38	10 up	lateral not letral
45	3 up	specimens not specimen
57	1	Time not strain
64	20	Volterra not Voltera

TABLE OF CONTENTS

LIST OF TABLES

LIST OF FIGURES

NOMENCLATURE

$A(\omega)$ Amplitude in the Cosine Fourier Transform

$B(\omega)$ Amplitude in the Sine Fourier Transform

E Young's Modulus

$\bar{E}$ $=E'+iE''$, Complex Modulus

E' Real Part of Complex Modulus

E'' Imaginary Part of Complex Modulus

$En(\omega)$ Energy of a wave over its period T_o

$G(\omega)$ Modulus in Complex Fourier Transform

$$[=(A^2(\omega)+B^2(\omega))^{1/2}]$$

$I(\omega)$ Intensity of a Wave of Frequency ω

$L(\omega)$ Reduction Coefficient

$L_{avg}(\omega)$ Average Reduction Coefficient

$F(u(t))$ $=U(\omega)$, Fourier Transform of $u(t)$ with respect to t

$F^{-1}(U(\omega))$ $=u(t)$, Iniverse Fourier Transform of $U(\omega)$ with

       respect to ω

T Time Duration of Pulse

T_o Time Period of a Wave of Frequency ω

c Elastic Wave Propagation Velocity

$\bar{c}$ Phase Velocity in Linear Viscoelastic Material

$f'(t-\frac{x}{c})$ Derivative with Respect to Argument $(=\dfrac{\partial f(t-\frac{x}{c})}{\partial (t-\frac{x}{c})})$

$\dot{f}$ Derivative with respect to Time

l Length of the Finite Bar in Three-Bar System

p Frequency of Half Sine Wave

t Time

u	Particle Displacement
$\dot{u}$	Particle Velocity
x	Distance from Origin
z	Impedance
z_0	Impedance of Semi-Infinite Bar in Three-Bar System
$\alpha_T(\omega)$	Transmission Coefficient at Frequency ω
ε	Strain
$\phi,\ \psi$	Phase Difference
λ_1	$=(z_0-z)/(z_0+z)$
λ_2	$=2z_0/(z_0+z)$
ν	Poisson's Ratio
ρ	Density
σ	Stress
$\bar{\sigma}$	$F(\sigma(t))$, Fourier Transform of $\sigma(t)$.
τ	Time taken by a Stress Wave to Travel the Length l of Finite Bar
ω	Circular Frequency

Superscripts i, r, t represent Incident, Reflected and Transmitted Pulse or Wave.

Subscripts 1, 2, 3 refer to bars 1, 2 and 3.

ACKNOWLEDGEMENT

1. INTRODUCTION

The problem of isolation of buildings and structures from acoustic noise and vibration is quite old. Lead-asbestos pads have been used [8] for the last forty-five years in the foundations of buildings to prevent transmission of vibrations from the ground into the buildings. Similarily lead also finds application in many other areas to control sound and vibrations [9].

The phenomenon of wave propagation in solid bars is well known. Experimental investigations were under way by the beginning of the 20th century. The "split Hopkinson pressure bar" method was introduced in mid 20th century to study the behaviour of small specimens under dynamic loading. Several methods have been employed in the past using explosive charge and mechanical devices to produce a pulse for dynamic compression testing of solids.

So far scientists have concentrated their attention towards dynamic compression testing of small specimen in order to study the dynamic behaviour of materials and to determine dynamic stress-strain curves, etc. Setups similar to split Hopkinson pressure bar-method were used. The present work is aimed at the study of the frequency dependence of materials, and their vibration isolation characteristics.

2. STATEMENT OF PROBLEM

The problem was to design and construct equipment adequate for the study of the frequency response of a material and to analyse the behaviour of the specimens of different lengths with a view to reducing the transmission of acoustic vibrations across them.

The above problem was divided into the following sub-problems:

i) Design and construct a system to produce stress pulses covering the acoustic frequency band, with small stress amplitudes;

ii) Set up instrumentation to record the observations of experiments conducted;

iii) Analyse the records to investigate the effects of specimen length and material properties on the specimen's capacity to reduce the amplitude of vibration transmitted across it.

3. REVIEW

3.1 Review of Theoretical Work

3.1.1 Wave Propagation in Elastic and Viscoelastic Bars

In 1807 Thomas Young gave laws governing the propagation of elastic waves in bars. The solution of the governing differential equation

$$\rho \frac{\partial^2 u}{\partial t^2} = E \frac{\partial^2 u}{\partial x^2} \qquad (3.1.1)$$

which is

$$u = f(t+\frac{x}{c}) + g(t-\frac{x}{c}) \ , \qquad (3.1.2)$$

where

$$c = \sqrt{E/\rho} \qquad (3.1.3)$$

describes the two waves $f(t+\frac{x}{c})$ and $g(t-\frac{x}{c})$ propagating with velocity c in the negative and positive x directions respectively.

Later H. Kolsky [1] analysed one-dimensional wave propagation in viscoelastic solids by introducing the concept of the complex elastic modulus for describing sinusoidal wave propagation. The complex modulus $\bar{E}$ is defined as the ratio of sinusoidally varying stress

$$\sigma = \sigma_0 \exp(i\omega t) \qquad (3.1.4)$$

to the sinusoidally varying strain

$$\epsilon = \epsilon_0 \exp(i\omega t - i\delta) . \qquad (3.1.5)$$

In (3.1.4) and (3.1.5) respectively, σ_0 and ϵ_0 are real. δ is the phase lag between the applied stress σ and the resultant strain ϵ. The complex modulus is then given by

$$\bar{E} = E' + iE'' = \frac{\sigma}{\epsilon} = \frac{\sigma_0}{\epsilon_0} \exp(i\delta) = E^* \exp(i\delta) \qquad (3.1.6)$$

where

$$E^* = [E'^2 + E''^2]^{1/2} \qquad (3.1.7)$$

and

$$\tan \delta = E''/E' . \qquad (3.1.8)$$

Hence for sinusoidally varying displacement

$$u = U(x)e^{i\omega t}$$

it follows from (3.1.6) that

$$\sigma = \bar{E} \frac{\partial u}{\partial x} . \qquad (3.1.9)$$

Replacing E in the equation of motion (3.1.1) by $\bar{E}$, yields, for sinusoidally varying displacement,

$$\bar{E} \frac{\partial^2 u}{\partial x^2} = \rho \frac{\partial^2 u}{\partial t^2} . \qquad (3.1.10)$$

The solution of (3.1.8) for a progressive sinusoidal wave of frequency $\omega/2\pi$, whose displacement at the origin is given by $u_o \exp(i\omega t)$, is

$$u = u_o \exp\left(-\alpha x + i\omega\left(t - \frac{x}{c}\right)\right) \tag{3.1.11}$$

where

$$\bar{c} = (E^*/\rho)^{1/2} \sec \frac{\delta}{2} \tag{3.1.12}$$

$$\alpha = (\omega/c) \tan \delta/2 . \tag{3.1.13}$$

The propagation of a pulse has been treated by Fourier synthesis and thus the displacement at the origin (x=0.0) is expressed as the Fourier integral

$$u(0,t) = \int_{-\infty}^{\infty} A(\omega)\exp(i\omega T)\,d\omega . \tag{3.1.14}$$

Therefore,

$$u(x,t) = \int_{-\infty}^{\infty} A(\omega)\exp\left(-\alpha x + i\omega\left(t - \frac{x}{c}\right)\right)d\omega \tag{3.1.15}$$

where $A(\omega)$ is a complex function of the frequency ω.

3.1.2 Wave form Produced by Mechanical Impact:

Various authors have analysed the problem of finding the length or duration of a stress pulse produced in a long bar by the impact between a stationary long bar and moving objects of different geometries.

Timoshenko [2] has shown that the length of the stress pulse produced by the longitudinal impact between two bars is $2l_1$, where l_1 is the length of the shorter bar.

Hertz [3] analysed the problem of a ball of radius r and mass m, striking a semi-infinite bar with velocity v_o. He derived the differential equation

$$\frac{d^2\alpha}{dt^2} + \frac{k}{\rho c_o \Omega} \frac{d\alpha^{3/2}}{dt} + \frac{k}{m} \alpha^{3/2} = 0 \qquad (3.1.16)$$

with the initial conditions $\alpha=0$ and $v=v_o$ for $t=0$, where α is the indentation of the impinging ball and Ω is the area of cross section of the bar. The constant k in (3.1.16) is given by

$$k = \frac{2}{3} \frac{E}{(1-\nu^2)} r^{1/2} \qquad (3.1.17)$$

where E, ρ and ν refer to the material of the bar.

The solution of (3.1.16) was found to be in close agreement with the experimental results [3].

W.A. Prowse [4] applied the Hertz theory to analyse the impact of a round-headed bar and found the expression

$$\beta = \frac{2\pi}{\sqrt{3}} + 2 \log \left[\frac{1+\delta+\delta^2}{(1-\delta)^2} \right] - 4\sqrt{3} \tan^{-1} \frac{2\delta+1}{\sqrt{3}} \qquad (3.1.18)$$

where

$$\delta = \left(\frac{\alpha}{\alpha_1}\right)^{3/2} ; \qquad \beta = \frac{6v_o}{\alpha_1} t ,$$

and α is the indentation at time t, α_1 is the maximum indentation, and v_o is the velocity of the impinging bar.

3.2 Review of Experimental Work

In 1914 Bertram Hopkinson [5] proposed an experimental technique, now known as the Hopkinson pressure bar method, for measuring the pressure produced by the impact of a projectile or explosive charge on the end of a long bar. The apparatus employed a short bar, called the time piece, stuck by means of grease to the end of a steel bar, several feet long, suspended horizontally by means of strings.

The pressure to be measured was applied at the end of the long steel bar, opposite to the end to which the time piece was attached. The time piece flew off when the pressure wave, reflected as tension wave from the end of the time piece, reached the junction of the time piece and the long steel bar. The momenta of time pieces of various lengths were recorded to calculate the pressure pulse.

In 1949, Kolsky [6] introduced the "split Hopkinson pressure bar" apparatus. This employed a disc specimen sandwiched between two long steel bars suspended horizontally by strings. An explosive charge at the end of the steel anvil bar caused a short duration ($\sim$1 micro-sec.) stress pulse in the anvil bar. The pulse suffered dispersion during propagation through bar due to the geometric and mechanical properties of the bar.

The displacement-time relationship was measured by a parallel plate condenser at the free end of the second bar. The

stress-time and strain-time relationships were derived by numerical analysis of the displacement-time relationships obtained in the absence and presence of the specimen.

Davies and Hunter (1962), [6], studied the mechanical behavior of solids under dynamic compression testing. Their method differed from Kolsky's mainly in specimen geometry. For Kolsky's specimen, since $a/h \approx 10$ (a is the radius and h is the thickness of the specimen), stresses in the tangential and radial directions arose due to frictional forces between the specimen-bar interfaces.

A criterion to indicate when frictional forces can be neglected, was derived by Hill in 1950, [6]. This criterion required $a/h << 25$ in the experiment conducted by Davies and Hunter, and this condition was satisfied.

The circular faces of bars and specimen in the Davies and Hunter experiments were finished to optical flatness. The specimens were held in position by "wrung joints."

In recent years the use of strain gages for measurements of strain pulses has been established. Experiments conducted by R.M. Davies, D.H. Edwards and D.E. Thomas in 1950 [7] led to the conclusion that static and dynamic gage factors are practically the same.

4. THEORY

In order to provide some theoretical basis to verify qualitatively the experimental investigations, the following analysis has been developed.

4.1 Propagation of a Longitudinal Stress Pulse in Coupled Bars

First of all, we consider the case of two semi-infinite bars of the same diameter but of different materials coupled together (Figure 4.1.1).

From (3.1.1) and (3.1.2) waves propagating in bars 1 and 2 may be described by

$$u_1 = f_1(t+\frac{x}{c_1})+g_1(t-\frac{x}{c_1}) \qquad\qquad (4.1.1)$$

$$u_2 = f_2(t+\frac{x}{c_2})+g_2(t-\frac{x}{c_2}) \ . \qquad\qquad (4.1.2)$$

Therefore particle velocity is given by

$$\dot{u}_1 = f_1{}'(t+\frac{x}{c_1}) + g_1{}'(t-\frac{x}{c_1}) \qquad\qquad (4.1.3)$$

$$\dot{u}_2 = f_2{}'(t+\frac{x}{c_2}) + g_2{}'(t-\frac{x}{c_2}) \ . \qquad\qquad (4.1.4)$$

Since the stress in elastic bar is related to strain by Hooke's law, the stress σ_1 and σ_2 are given by

$$\sigma_1 = \frac{E_1}{c_1} f_1{}'(t+\frac{x}{c_1}) - \frac{E_1}{c_1} g_1{}' (t-\frac{x}{c_1}) \qquad\qquad (4.1.5)$$
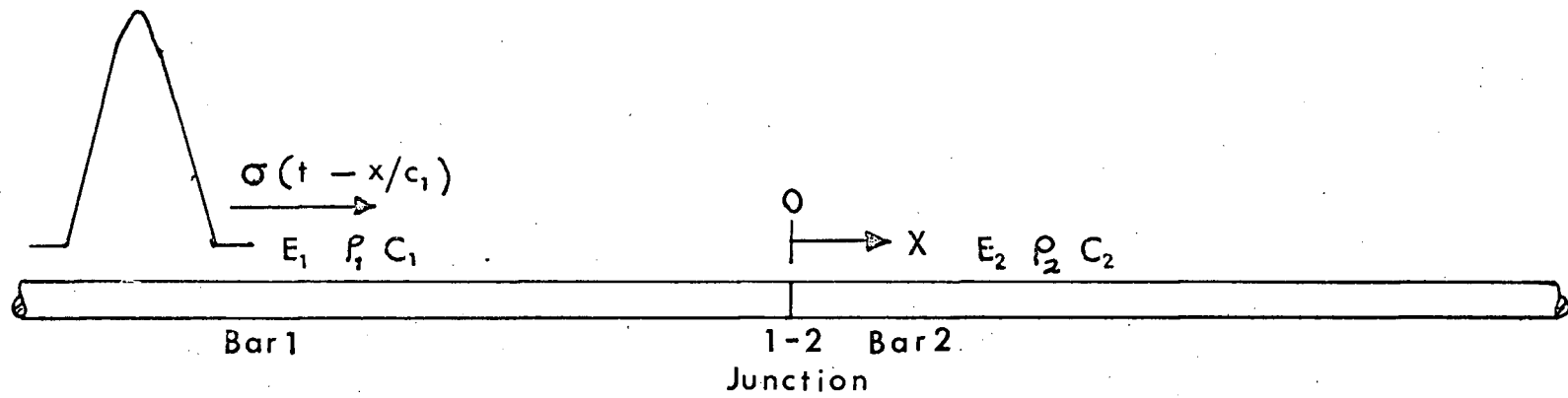
Figure 4.1.1   Two-Bar System

$$\sigma_2 = \frac{E_2}{c_2} f_2'(t+\frac{x}{c_1}) - \frac{E_2}{c_2} g_2'(t-\frac{x}{c_2}) \quad . \qquad (4.1.6)$$

An incident stress wave given by

$$\sigma_1{}^i = \sigma(t-\frac{x}{c_1})$$

is considered to travel in the positive x direction in bar 1
and to arrive at the junction x=0.0 at time t=0.

Therefore, in (4.1.5)

$$f_1'(t+\frac{x}{c_1}) = 0 \qquad \text{for } t<0 \qquad (4.1.7)$$

and

$$g_1'(t-\frac{x}{c_1}) = -\frac{c_1}{E_1} \sigma(t-\frac{x}{c_1}) \quad . \qquad (4.1.8)$$

As there is no wave travelling in negative x direction
in bar 2,

$$f_2'(t+\frac{x}{c_2}) = 0 \qquad (4.1.9)$$

Continuity of stress and particle velocity requires,
at x=0.0,

$$\left.\begin{array}{l} \sigma_1 = \sigma_2 \\[4pt] \dot{u}_1 = \dot{u}_2 \end{array}\right\} \qquad (4.1.10)$$

The boundary conditions (4.1.10) for t>0 applied to
(4.1.3), (4.1.4), (4.1.5), (4.1.6) yield the set of equations

$$f_1{}'(t) + g_1{}'(t) = f_2{}'(t) + g_2{}'(t)$$

$$\} \quad (4.1.11)$$

$$\frac{E_1}{c_1} f_1{}'(t) - \frac{E_1}{c_1} g_1{}'(t) = \frac{E_2}{c_2} f_2{}'(t) - \frac{E_2}{c_2} g_2{}'(t) \ .$$

Solving (4.1.11) together with (4.1.8) and (4.1.9) (for x=0.0), for $g_1{}'$ and $f_2{}'$ and then substituting these expressions in (4.1.5) and (4.1.6) yields $\sigma_1(x,t)$ and $\sigma_2(x,t)$ given by the expressions,

$$\sigma_1(x,t) = \sigma(t - \frac{x}{c_1}) + \frac{z_2 - z_1}{z_2 + z_1} \sigma(t + \frac{x}{c_1}) \ , \qquad (4.1.12)$$

where the reflected wave in bar 1 is

$$\sigma_1{}^r(x,t) = \frac{z_2 - z_1}{z_2 + z_1} \sigma(t + \frac{x}{c_1}) \ , \qquad (4.1.13)$$

and transmitted wave in bar 2.

$$\sigma_2{}^t(x,t) = \sigma_2(x,t) = \frac{2z_2}{z_2 + z_1} \sigma(t - \frac{x}{c_2}) \qquad (4.1.14)$$

The impedances z_1 and z_2 of bar 1 and bar 2 respectively are given by

$$z_1 = \rho_1 c_1 = E_1/c_1 \quad \text{and} \quad z_2 = \rho_2 c_2 = E_2/c_2 \ . \qquad (4.1.15)$$

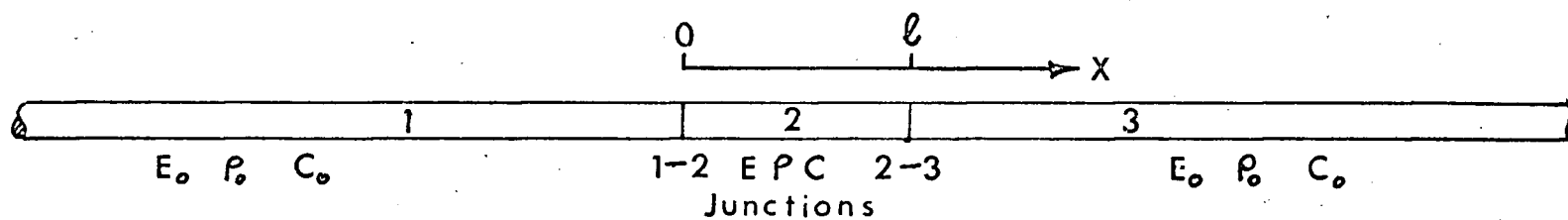The above analysis shows that phenomena of reflection and

Figure 4.1.2   Three-Bar System

transmission take place at the junction, when the incident wave reaches the junction between two bars.

In another example, an elastic bar of length 1 is sandwiched between two semi-infinite bars (Figure 4.1.2). The semi-infinite bars are of the same material, with physical properties E_o, ρ_o and c_o. The finite bar is of different material with physical properties E, ρ and c.

We now define

$$\tau = 1/c$$
$$\lambda_1 = (z_o-z)/(z_o+z) \ .$$

Then   (4.1.16)

$$(1+\lambda_1) = 2z_o/(z_o+z) = \lambda_2$$

and

$$(2-\lambda_2) = (1-\lambda_1) = 2z/(z_o+z) \ .$$

A stress wave in the form of a Heaviside step function, given by

$$\sigma_1^i(x,t) = \sigma(t-\frac{x}{c_1}) = h(t-\frac{x}{c_1}) \qquad (4.1.17)$$

is assumed to travel in bar 1. Beginning at time t=0 when it arrives at the junction between bar 1 and bar 2, it is partly reflected and partly transmitted to bar 2. The wave transmitted to bar 2, when it arrives at the junction 2-3, is partly reflected and partly transmitted to bar 3. Thus stress waves travel back and forth in bar 2 and give rise to successive reflection and transmission at junctions 1-2 and 2-3.

From (4.1.12), (4.1.14) and (4.1.16), the analysis has

Bar 1 | Bar 2 | Bar 3

$h(t - x/c_0)$

$h(t + x/c_0)$

$(2-\lambda_2) h(t - x/c)$

$(2-\lambda_2)\lambda_1 h(t - \tau + x/c)$

$(2-\lambda_2)\lambda_2 h(t - \tau - x/c_0)$

$(2-\lambda_2)\lambda_2\lambda_1 h(t - 2\tau + x/c_0)$

$(2-\lambda_2)\lambda_1^2 h(t - 2\tau - x/c)$

$(2-\lambda_2)\lambda_1^3 h(t - 3\tau + x/c)$

$(2-\lambda_2)\lambda_2\lambda_1^2 h(t - 3\tau - x/c_0)$

$(2-\lambda_2)\lambda_2\lambda_1^3 h(t - 4\tau + x/c_0)$

$(2-\lambda_2)\lambda_1^4 h(t - 4\tau - x/c)$

$(2-\lambda_2)\lambda_2\lambda_1^4 h(t - 5\tau - x/c_0)$

$(2-\lambda_2)\lambda_2\lambda_1^{2n-1} h(t - 2n\tau + x/c_0)$

$(2-\lambda_2)\lambda_1^{2n} h(t - 2n\tau - x/c)$

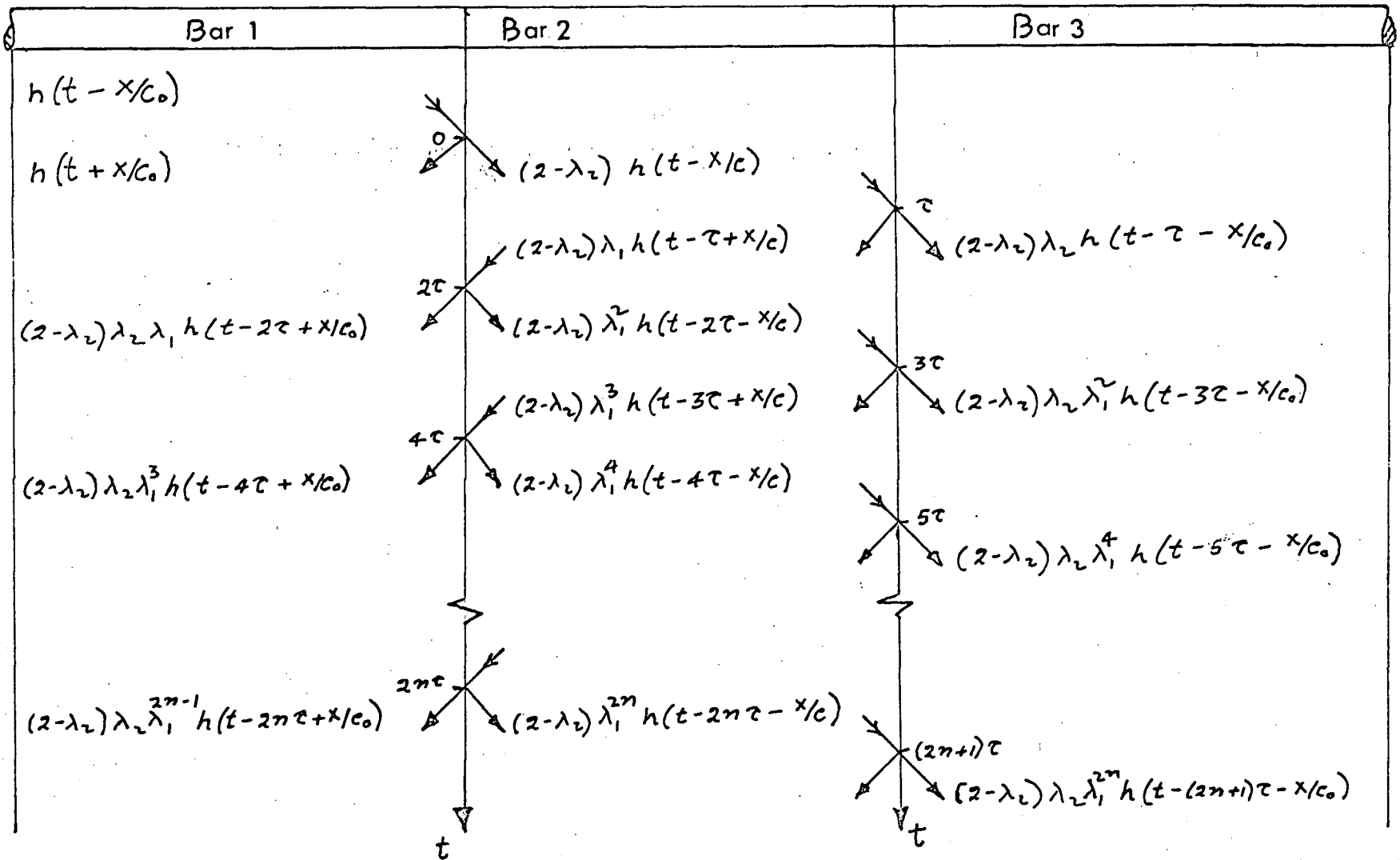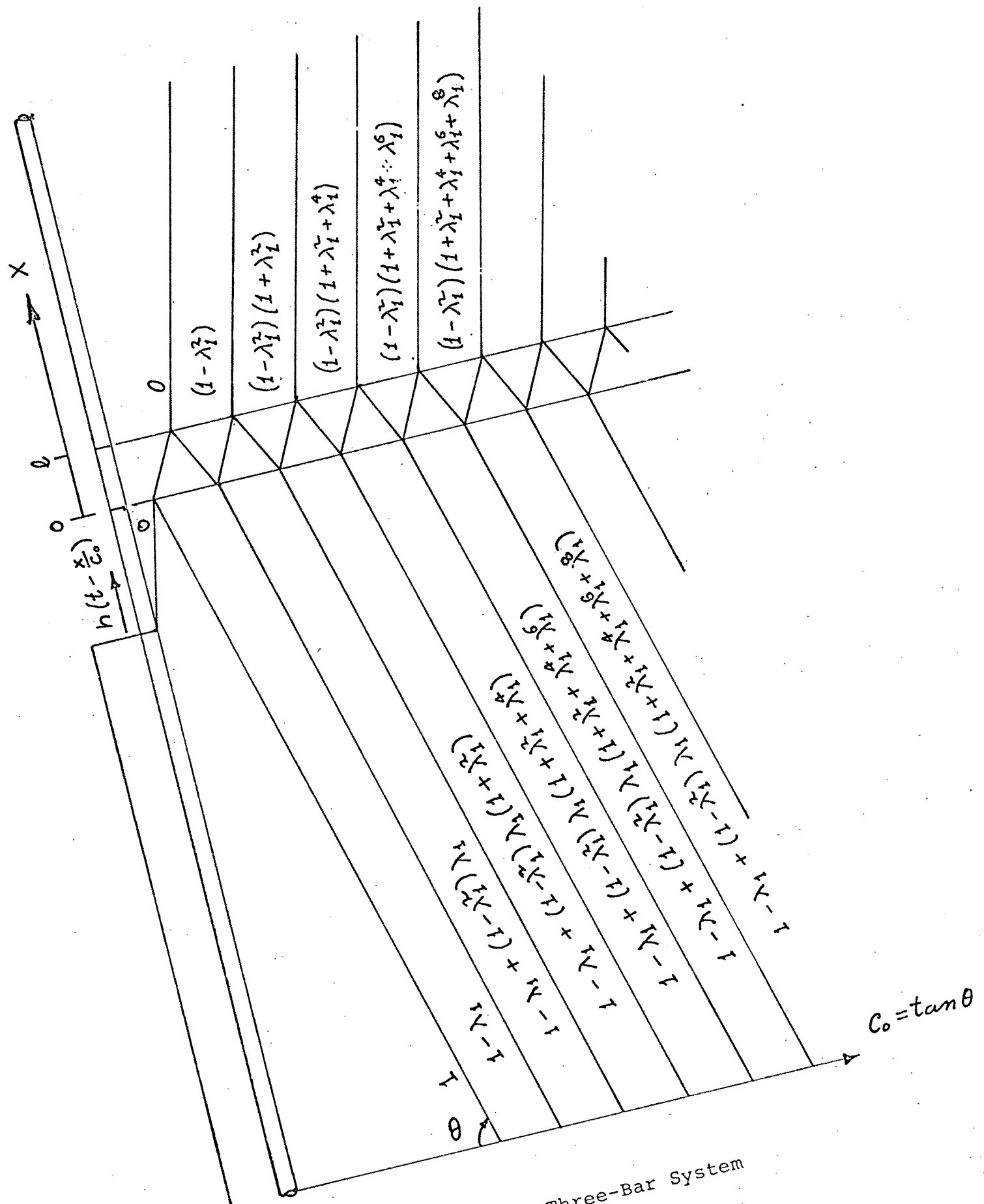$(2-\lambda_2)\lambda_2\lambda_1^{2n} h(t - (2n+1)\tau - x/c_0)$

TABLE 4.1.A

STRESS-TIME-DISTANCE RELATIONSHIP FOR SUCCESSIVE REFLECTION AND TRANSMISSION FOR AN
ELASTIC BAR SANDWICHED BETWEEN TWO SEMI-INFINITE ELASTIC BARS

Figure 4.1.3   σ-x-t Plot: Three-Bar System

been carried out to develop the stress-time-distance relation-
ships and results for successive reflection and transmission
are shown in the Table (4.1.A) and Figure 4.1.3.

The stresses in bars 1 and 3, $\sigma_1(x,t)$ and $\sigma_3(x,t)$ re-
spectively can be obtained by superposition of the stresses
listed in Table (4.1.A).

Thus

$$\sigma_1(x,t) = h(t-\frac{x}{c_o})-\lambda_1 h(t+\frac{x}{c_o})+(1-\lambda_1^2)\lambda_1[h(t-2\tau+\frac{x}{c_o})$$

$$\text{(4.1.18)}$$

$$+\lambda_1^2 h(t-4\tau+\frac{x}{c_o})+\ldots+\lambda_1^{2(n-1)}h(t-2n\tau+\frac{x}{c_o})+\ldots]$$

and,

$$\sigma_3(x,t) = (1-\lambda_1^2)[h(t-\tau-\frac{x}{c_o}) + \lambda_1^2 h(t-3\tau-\frac{x}{c_o})+\lambda_1^4 h(t-5\tau-\frac{x}{c_o})$$

$$+\ldots+\lambda_1^{2(n-1)}h(t-(2n-1)\tau-\frac{x}{c_o})+\ldots] . \qquad \text{(4.1.19)}$$

Then $\sigma_1(x,t)$ can be expressed as

$$\sigma_1(x,t) = \sigma_1^i(x,t)+\sigma_1^r(x,t) \qquad \text{(4.1.20)}$$

where $\qquad\qquad\qquad\qquad\qquad\qquad\qquad\qquad\qquad$ (4.1.20)

$$\sigma_1^i(x,t) = h(t-\frac{x}{c_o})$$

is the incident wave travelling in the positive x direction, and
$\sigma_1^r(x,t)$ is the reflected wave travelling in the negative x
direction in bar 1 after time t=0. The stress $\sigma_3(x,t)$ in bar 3
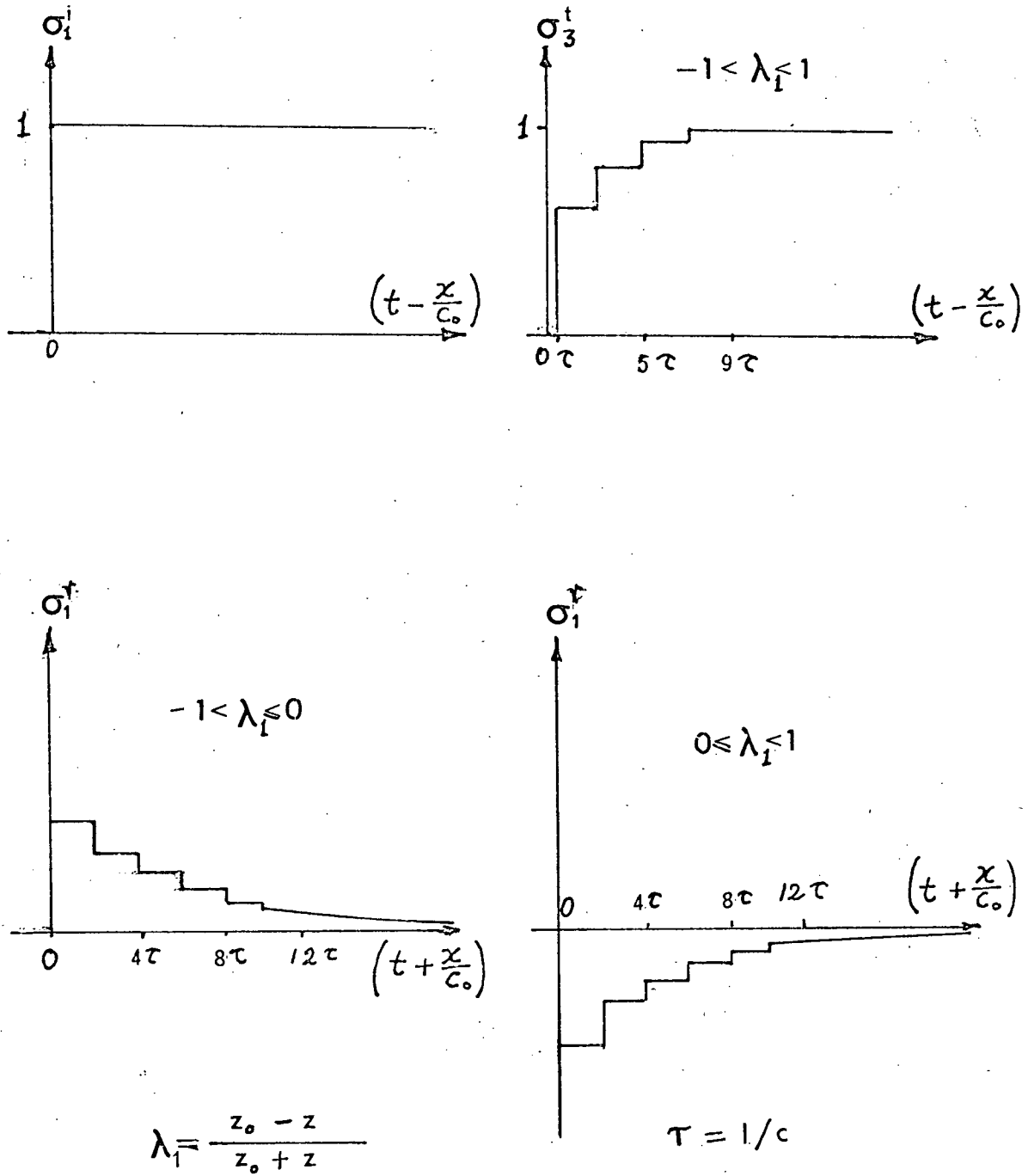is associated with a transmitted wave $\sigma_3^t(x,t)$ travelling in

Figure 4.1.4 Incident Reflected and Transmitted Waves in Three-Bar System

positive x direction in bar 3 when t>0. The waves σ_1^i, σ_1^r

and σ_1^i, σ_1^r and σ_3^t are plotted in Figure 4.1.4, which shows

the form of the incident reflected and transmitted waves.

Now we investigate the problem of propagation of an

incident rectangular pulse of duration T (Figure 4.1.5a) propa-

gating in the positive x direction in bar 1 in a three-bar

system (Figure 4.1.2).

The rectangular pulse can be expressed as

$$\sigma_1^i(x,t) = h(t-\frac{x}{c_o}) - h(t-T-\frac{x}{c_o}) \quad .$$

Thus $\sigma_1^r(x,t)$ and $\sigma_3^t(x,t)$, the reflected and transmitted waves

respectively, can be obtained by superposition of the reflected

and transmitted waves for $h(t-\frac{x}{c_o})$ and $h(t-T-x/c_o)$ using (4.1.18)

and (4.1.19).

The results for a particular case (T=4τ) have been der-

ived systematically in Figure 4.1.5 and Figure 4.1.6 by the

superposition of waves shown in Figure 4.1.4 and Figure 4.1.3.

The following analysis has been carried out for a finite

viscoleastic bar sandwiched between two semi-infinite elastic

bars of the same material (Figure 4.1.7). The incident, trans-

mitted and reflected displacement pulses are given as

$$u_1^i(x,t) = f_1(t-\frac{x}{c_o}) \text{ and } u_1^r(x,t) = g_1(t+\frac{x}{c_o})$$

$$u_3(x,t) = u_3^t(x,t) = f_3(t-\frac{x}{c_o}) \qquad (4.1.21)$$

$$u_1(x,t) = f_1(t-\frac{x}{c_o}) + g_1(t+\frac{x}{c_o}) \quad .$$
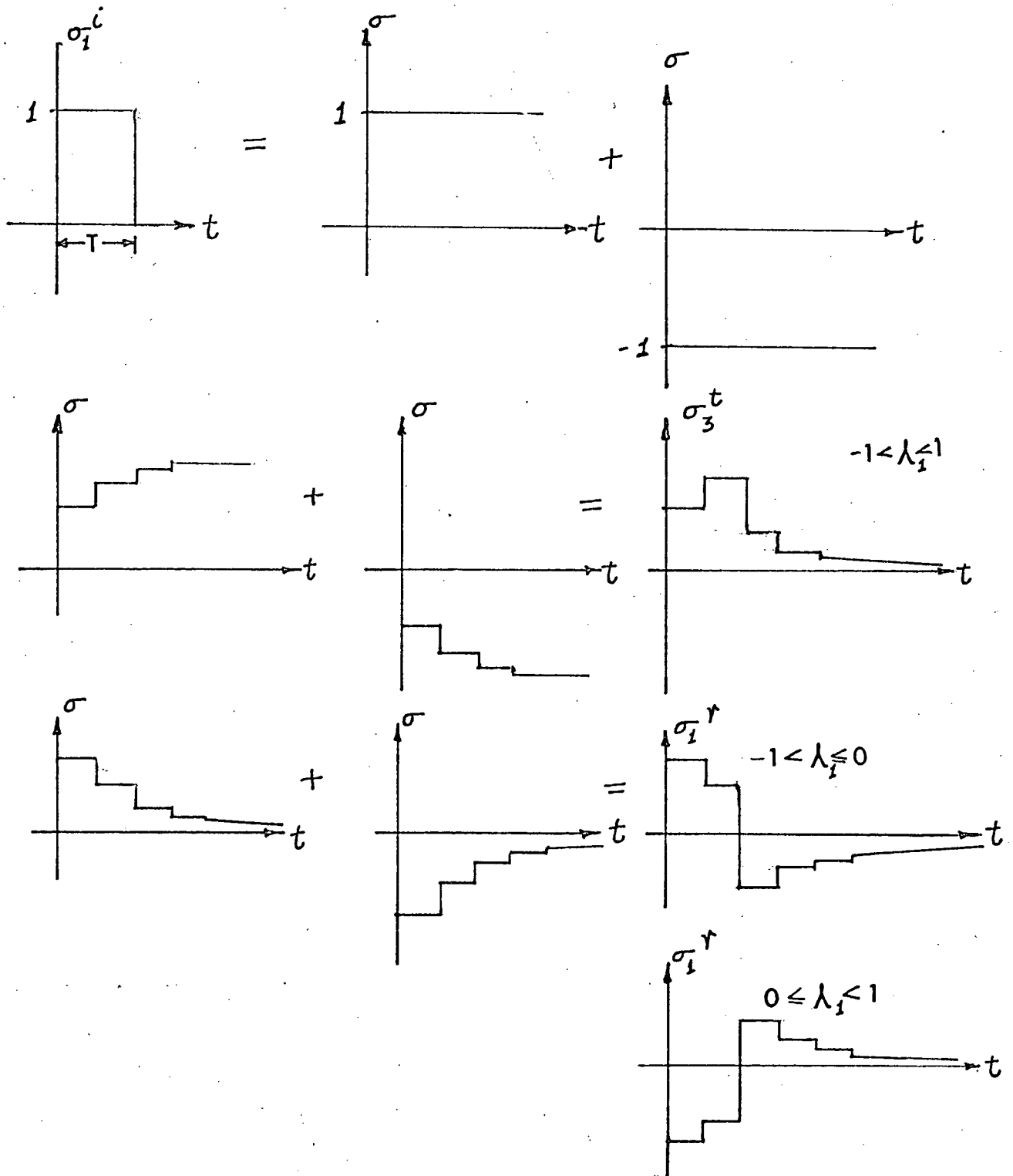
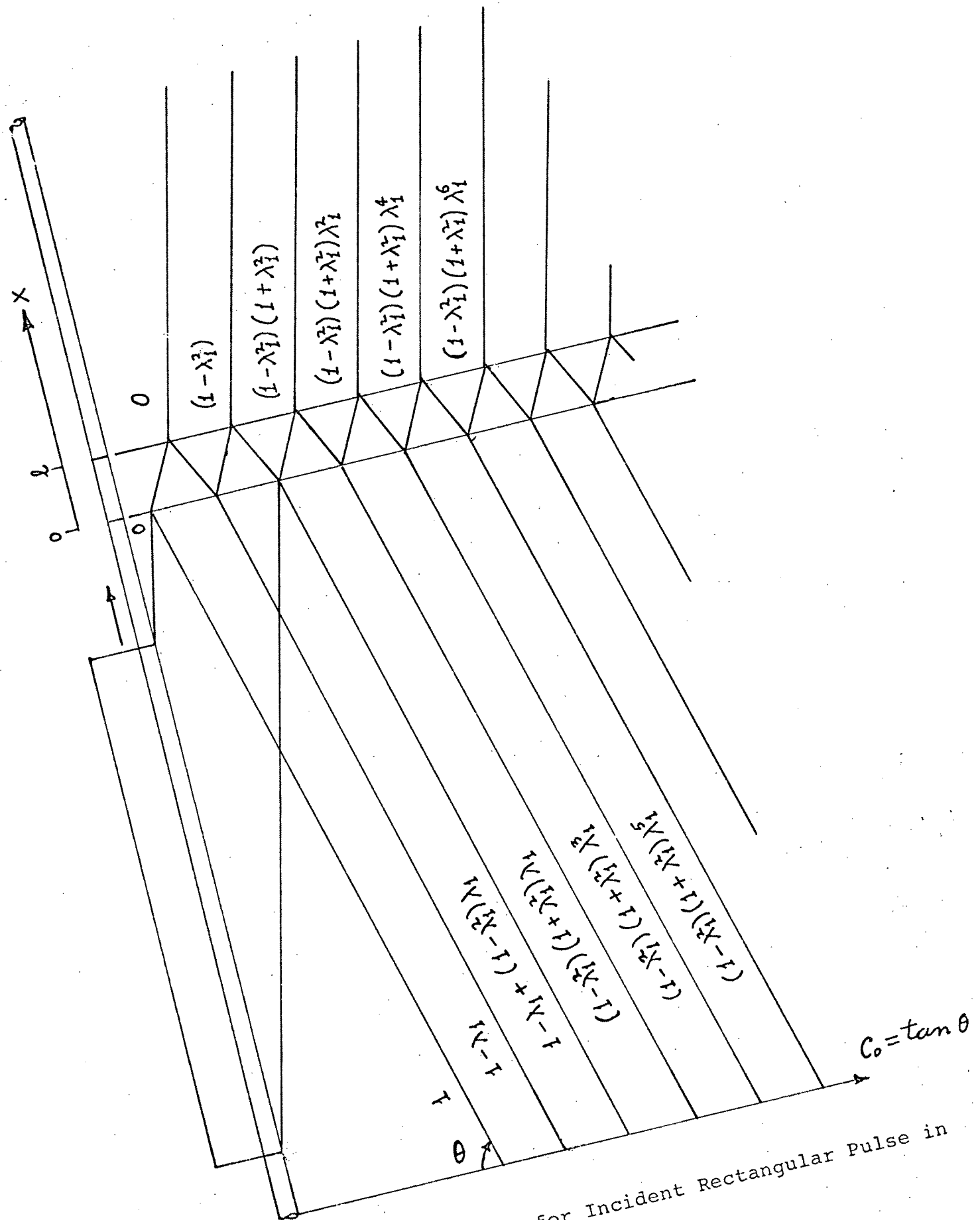Figure 4.1.5   Propagation of Rectangular Pulse in Three-Bar
System

Figure 4.1.6 σ-X-t Plot for Incident Rectangular Pulse in
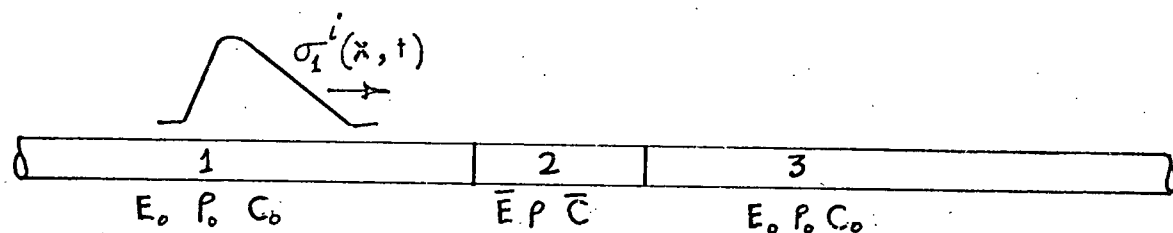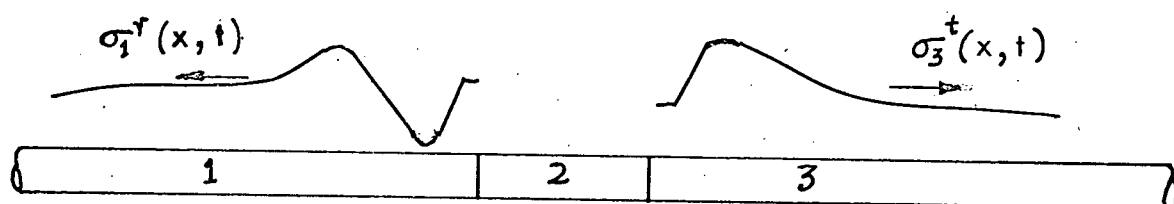Three-Bar System

(a)   For $t < 0$

(b)   For $t \rightarrow \infty$

Figure 4.1.7   Viscoelastic Bar Coupling Two Elastic
Bars

Fourier transforms are defined as,

$$F^{-1}[F(\omega)] = f(t) = \frac{1}{\sqrt{2\pi}} \int_{-\infty}^{\infty} F(\omega) e^{-i\omega t} \, d\omega \qquad (4.1.22)$$

$$F[f(t)] = F(\omega) = \frac{1}{\sqrt{2\pi}} \int_{-\infty}^{\infty} f(t) \, e^{i\omega t} \, dt \qquad (4.1.23)$$

$$\dot{f}(t) = \frac{1}{\sqrt{2\pi}} \int_{-\infty}^{\infty} (-i\omega) F(\omega) \, e^{-i\omega t} \, d\omega \quad . \qquad (4.1.24)$$

Therefore,

$$F(\dot{f}(t)) = -i\omega F(\omega)$$

and

$$F(\ddot{f}(t)) = -\omega^2 F(\omega)$$

The equation for sinusoidal wave propagation in bar 2 can be written as

$$\frac{\partial^2 u_2}{\partial x^2} - \frac{1}{\bar{c}^2} \frac{\partial^2 u_2}{\partial t^2} = 0, \quad 0 \leqslant x \leqslant 1 \qquad (4.1.26)$$

where

$$\bar{c}^2 = \frac{E' + iE''}{\rho}$$

for viscoelastic materials. For the special case when bar 2 is elastic, $\bar{c}$ is replaced by $c = \sqrt{E/\rho}$. Applying the Fourier transformation to (4.1.26) yields

$$U_2''(\omega) + \frac{\omega^2}{\bar{c}^2} U_2(\omega) = 0 \quad . \qquad (4.1.27)$$

The solution of (4.1.27) may be written

$$U_2(\omega) = P(\omega) \cos \frac{\omega x}{c} + Q(\omega)\sin \frac{\omega x}{c} \; . \qquad (4.1.28)$$

The inverse Fourier transformation yields,

$$u_2(x,t) = \frac{1}{\sqrt{2\pi}} \int_{-\infty}^{\infty} [P(\omega)\cos \frac{\omega x}{c} + Q(\omega)\sin \frac{\omega x}{c}]e^{-i\omega t} \, d\omega$$

$$(4.1.29)$$

At x=0,

$$u_2(0,t) = \frac{1}{\sqrt{2\pi}} \int_{-\infty}^{\infty} P(\omega)e^{-i\omega t} \, d\omega \qquad (4.1.30)$$

$$\dot{u}_2(0,t) = \frac{1}{\sqrt{2\pi}} \int_{-\infty}^{\infty} (-i\omega) \, P(\omega)e^{-i\omega t} \, d\omega \qquad (4.1.31)$$

$$u_2'(0,t) = \frac{1}{\sqrt{2\pi}} \int_{-\infty}^{\infty} \frac{\omega}{c} \, Q(\omega)e^{-i\omega t} \, d\omega \qquad (4.1.32)$$

The requirement of continuity of stress and particle velocity at the junctions (x=0 and x=1) yields the following equations:

$$-\frac{E_o}{c_o} f_1'(t) + \frac{E_o}{c_o} g_1'(t) = \frac{1}{\sqrt{2\pi}} \int_{-\infty}^{\infty} \frac{\omega}{c} \, \bar{E} \, Q(\omega)e^{-i\omega t} d\omega \qquad (4.1.34)$$

$$f_1'(t) + g_1'(t) = \frac{1}{\sqrt{2\pi}} \int_{-\infty}^{\infty} (-i\omega)P(\omega)e^{-i\omega t} \, d\omega \qquad (4.1.34)$$

$$\dot{u}_2(1,t) = f_3'(t - \frac{1}{c_o}) \qquad (4.1.35)$$

$$-\frac{E_o}{c_o} f_3'(t - \frac{1}{c_o}) = \frac{1}{\sqrt{2\pi}} \int_{-\infty}^{\infty} \frac{\omega \bar{E}}{c} \, [-P(\omega)\sin \frac{\omega 1}{c} + Q(\omega)\cos \frac{\omega 1}{c}]e^{-i\omega t} d\omega \; .$$

$$(4.1.36)$$

Combining and simplifing (4.1.35), (4.1.36) and (4.1.29)

yields

$$- \frac{E_o}{c_o} (-i\omega)[P(\omega)\cos \frac{\omega l}{\bar{c}} + Q(\omega)\sin \frac{\omega l}{\bar{c}}]$$

$$= \frac{\omega \bar{E}}{\bar{c}} [-P(\omega)\sin \frac{\omega l}{\bar{c}} + Q(\omega)\cos \frac{\omega l}{\bar{c}}]$$

or

$$[\cos \frac{\omega l}{\bar{c}} - \frac{ic_o\bar{E}}{\bar{c}E_o} \sin \frac{\omega l}{\bar{c}}] P(\omega) + [\sin \frac{\omega l}{\bar{c}} + \frac{ic_o\bar{E}}{\bar{c}E_o} \cos \frac{\omega l}{\bar{c}}]Q(\omega)=0 \ .$$

$$(4.1.37)$$

From (4.1.21), it can be shown that

$$- \frac{E_o}{c_o} f_3'(t-\frac{x}{c_o}) = \sigma_3{}^t(x,t), \qquad (4.1.38)$$

hence in conjunction with the Fourier transform of (4.1.35),
we obtain the equation

$$i\omega[P(\omega)\cos \frac{\omega l}{\bar{c}} + Q(\omega) \sin \frac{\omega l}{\bar{c}}] = \frac{c_o}{E_o} \bar{\sigma}_3{}^t (\omega) \ . \qquad (4.1.39)$$

Similarly, by (4.1.33) and (4.1.34), it can be shown that

$$i\omega \frac{E_o}{c_o} P(\omega) + \omega\frac{\bar{E}}{\bar{c}} Q(\omega) = 2\bar{\sigma}_1{}^i(\omega) \ . \qquad (4.1.40)$$

$P(\omega)$ and $Q(\omega)$ can be found from (4.1.37) and (4.1.40)
and hence $\sigma_3{}^t(x,t)$ and $\sigma_1{}^r(x,t)$ can be computed. Since the
values for $\bar{c}(\omega)$ are not available readily, (4.1.37), (4.1.39)

and (4.1.40) can be solved to give the following equation:

$$\sin \frac{\omega l}{\bar{c}} + 2i \left(\frac{\rho \bar{c}}{\rho_o c_o}\right) \cos \frac{\omega l}{\bar{c}} + \left(\frac{\rho \bar{c}}{\rho_o c_o}\right)^2 \sin \frac{\omega l}{\bar{c}} = 2i \left(\frac{\rho \bar{c}}{\rho_o c_o}\right) \frac{\bar{\sigma}_1{}^i}{\bar{\sigma}_3{}^t}$$

(4.1.41)

When $\sigma_1{}^i(x,t)$ and $\sigma_3{}^t(x,t)$ are known, $\bar{c}(\omega)$ can be found by solving (4.1.41). Then, since

$$\bar{E} = E' + iE'' = \rho [\bar{c}(\omega)]^2$$

the complex modulus of the material of bar 2 can be found.

4.2 Duration of Stress Pulse

The following analysis has been carried out to show the effect of the duration of a pulse on its frequency spectrum.

The frequency spectrum of a pulse $\sigma(t)$ is expressed by its Fourier transform. $\sigma(t)$ can be written as

$$\sigma(t) = \frac{1}{\pi} \int_o^\infty [A(\omega) \cos \omega t + B(\omega) \sin \omega t] \, d\omega$$

$$= \frac{1}{\pi} \int_o^\infty G(\omega) \sin(\omega t + \phi) d\omega$$

(4.2.1)

where

$$G(\omega) = [A^2(\omega) + B^2(\omega)]^{1/2}$$

(4.2.2)

is the modulus in the complex Fourier transform, and

$$\phi = \tan^{-1} [A(\omega) / B(\omega)]$$

(4.2.3)

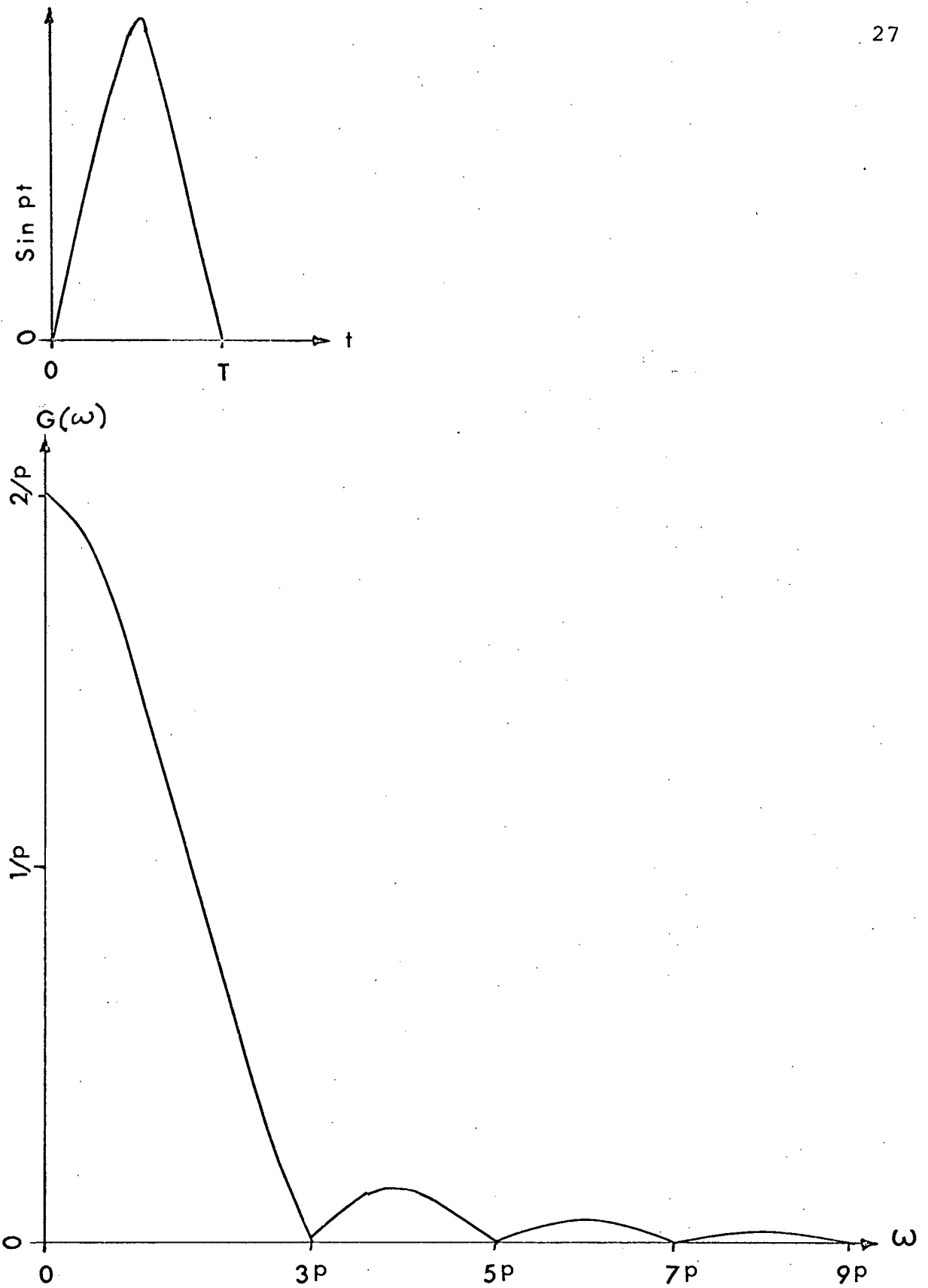is the argument in the complex Fourier transform

Figure 4.2.1   Fourier Transform for a Half Sine Wave

Also,

$$A(\omega) = \int_{-\infty}^{\infty} \sigma(t) \cos \omega t \, dt \qquad (4.2.4)$$

and

$$B(\omega) = \int_{-\infty}^{\infty} \sigma(t) \sin \omega t \, dt \quad . \qquad (4.2.5)$$

For the particular case of a stress pulse of the form of a half sine wave given by

$$\sigma(t) = \sin pt \quad \text{for } 0 \leqslant t \leqslant T$$
$$= 0 \qquad \text{for } 0 \geqslant t \geqslant T$$

where

$$p = \pi/T,$$

$A(\omega)$, $B(\omega)$ and $G(\omega)$ have been calculated as follows:

From (4.2.4)

$$A(\omega) = \int_{o}^{T} \sin pt \cos \omega t \, dt$$

$$\qquad (4.2.6)$$

$$= \frac{p}{p^2 - \omega^2} [1 + \cos \frac{\omega T}{2}]$$

and from (4.2.5)

$$B(\omega) = \int_{o}^{T} \sin pt \sin \omega t \, dt$$

$$= \frac{p}{p^2 - \omega^2} \sin \frac{\omega T}{2} \qquad \text{for } \omega \neq p \quad . \qquad (4.2.7)$$

Therefore, according to (4.2.2)

$$G(\omega) = \frac{2p}{p^2-\omega^2} \cos \frac{\pi\omega}{2p} \quad . \tag{4.2.8}$$

$G(\omega)$ has been plotted against frequency in Figure 4.2.1. Figure 4.2.1 shows that the amplitude (the modulus in the complex Fourier Transform), for $\omega > 2.5p$, is less than 20% of the maximum value at $\omega=0$. Hence to cover a larger frequency band a pulse of shorter duration would be required.

4.3 Momentum Analysis

By the law of conservation of linear momentum, the momentum of the incident pulse should be equal to the algebraic sum of the momenta of the reflected and the transmitted pulses. The momentum of the incident pulse is

$$M_1^i = \int_{-\infty}^0 \dot{u}\rho_0 dx = \int_{-\infty}^0 \dot{u}_1^i \rho_0 c_0 dt \tag{4.3.1}$$

and the total momentum of the reflected and transmitted pulses is

$$M_1^r + M_3^t = \int_0^\infty \dot{u}\rho_0 dx = \int_0^\infty \dot{u}_1^r \rho_0 c_0 dt + \int_0^\infty \dot{u}_3^t \rho_0 c_0 dt \tag{4.3.2}$$

Since $M_1^i = M_1^r + M_3^t$,

it follows that

$$\int_{-\infty}^0 \dot{u}_1^i dt = \int_0^\infty \dot{u}_1^r dt + \int_0^\infty \dot{u}_3^t dt \quad . \tag{4.3.3}$$

The incident and transmitted pulses are travelling in the positive x direction, and the reflected pulse in the negative x direction.

Then

$$u_1^i = g_1(t-\frac{x}{c_o}), \quad \text{and} \quad \dot{u}_1^i = g_1{}'(t-\frac{x}{c_o}) = -\frac{c_o}{E_o} \sigma_1^i(x,t)$$

$$u_1^r = f_1(t+\frac{x}{c_o}), \quad \text{and} \quad \dot{u}_1^r = f_1{}'(t+\frac{x}{c_o}) = \frac{c_o}{E_o} \sigma_1^r(x,t) \quad (4.3.4)$$

$$u_2^t = g_3(t-\frac{x}{c_o}), \quad \text{and} \quad \dot{u}_3^t = g_3{}'(t-\frac{x}{c_o}) = -\frac{c_o}{E_o} \sigma_3^t(x,t).$$

In view of (4.3.4), (4.3.3) may be written,

$$\int_{-\infty}^{o} \sigma_1^i(x,t)dt = -\int_{o}^{\infty} \sigma_1^r(x,t)dt + \int_{o}^{\infty} \sigma_3^t(x,t)dt, \quad (4.3.5)$$

which shows that the area under the stress-time curve of the incident pulse is equal to the corresponding area of reflected pulse substracted from the area of the transmitted pulse.

Examination of (4.2.4), (4.2.5) and (4.2.2) for $\omega=0$ shows that

$$G(0) = \int_{-\infty}^{\infty} \sigma(t)dt \quad (4.3.6)$$

and hence by (4.3.5)

$$G^i(0) = G^r(0) + G^t(0) \ . \qquad\qquad (4.3.7)$$

For an elastic three-bar system, it was proved analytically for the case of the propagation of the rectangular pulse of duration $T=4\tau$ and unit height, discussed in section 4.1, that

$$\int_o^\infty \sigma_1^{\ i}(t)\,dt = \int_o^T \sigma_1^{\ i}(t)\,dt = 4\tau$$

$$\int_o^\infty \sigma_1^{\ r}(t)\,dt = 0$$

and $\qquad \displaystyle\int_o^\infty \sigma_3^{\ t}(t)\,dt = 4\tau \ .$

Hence (4.3.5) is satisfied.

A similar check was made for the case when bar 2 is viscoelastic. In the limit as ω approaches zero (4.1.37) becomes

$$\frac{E_o}{c_o}\, P(\omega) + \frac{i\bar{E}}{\bar{c}}\, Q(\omega) = 0$$

or $\qquad\qquad\qquad\qquad\qquad\qquad\qquad\qquad\qquad (4.3.8)$

$$Q(\omega) = \frac{i\bar{c}E_o}{c_o\bar{E}}\, P(\omega) \ .$$

Substitution in (4.1.40) yields, when ω approaches zero,

$$[\frac{i\omega E_o}{c_o} + \frac{i\bar{c}E_o}{c_o\bar{E}}\, \omega\, \frac{\bar{E}}{\bar{c}}]\, P(\omega) = 2\bar{\sigma}_1^{\ i}(\omega)$$

or

$$\frac{i\omega E_o}{c_o} P(\omega) = \bar{\sigma}_1^i(\omega) \ .$$ (4.3.9)

By (4.1.39),

$$\frac{i\omega E_o}{c_o} P(\omega) = \bar{\sigma}_3^t(\omega)$$ (4.3.10)

and therefore,

$$\int_o^T \sigma_1^i(t)dt = \int_o^\infty \sigma_3^t(t)dt \ .$$ (4.3.11)

Solving (4.1.33) and (4.1.34) for the reflected pulse yields

$$-i\omega\frac{E_o}{c_o} P(\omega) + \omega\frac{\bar{E}}{\bar{c}} Q(\omega) = 2\bar{\sigma}_1^r(\omega)$$

or (4.3.12)

$$\bar{\sigma}_1^r(\omega) = [-i\omega\frac{E_o}{c_o} + \omega \frac{\bar{E}}{\bar{c}} \ i \frac{\bar{c}}{\bar{E}} \frac{E_o}{c_o}] P(\omega) \ .$$

$P(\omega)$ and $Q(\omega)$ are finite for $\omega=0$, provided the displacement $u_2(0,t)$ and the strain $u_2'(0,t)$ are integrable over the interval $-\infty<T<\infty$. Therefore as

$$\omega \to 0, \ \bar{\sigma}_1^r(\omega) \to 0 \ ,$$

hence (4.3.13)

$$\int_o^\infty \sigma_1^r(t)dt = 0 \ .$$

Thus (4.3.5) or (4.3.7) are satisfied from the results of (4.3.11) and (4.3.13).

5. EXPERIMENTATION AND INSTRUMENTATION

The present section deals with the design aspects of the experimental setup, and certain experiments carried out to arrive at the final design.

The split Hopkinson pressure bar apparatus introduced by Kolsky [6] was the basis for the design of the experimental setup. Changes were introduced to take account of the present requirements.

5.1 Experimental Setup

A schematic diagram of the setup is shown in Figure 5.1.1. The overall design consists of two main systems described as follows.

5.1.1 Mechanical System:

Two 0.25 in. diameter steel bars of lengths 4.0 ft. and 5.0 ft. were suspended by strings and the specimen to be tested was bonded between the two bars with paint. The incident pulse was introduced at free end of the 4.0 ft. long bar by the impact of a round-headed steel bar (1.5 in. long and 0.25 in. diameter) held loosely in a bronze bushing at the end of a pendulum.

5.1.2 Transducer and Recording System:

Budd strain gages (type C6-121 Budd Metafilm strain gages, red colour) were employed for the purpose of sensing the incident, reflected and transmitted pulses travelling in bar 1 and bar 3. The gage on bar 1 was mounted 18 in. away
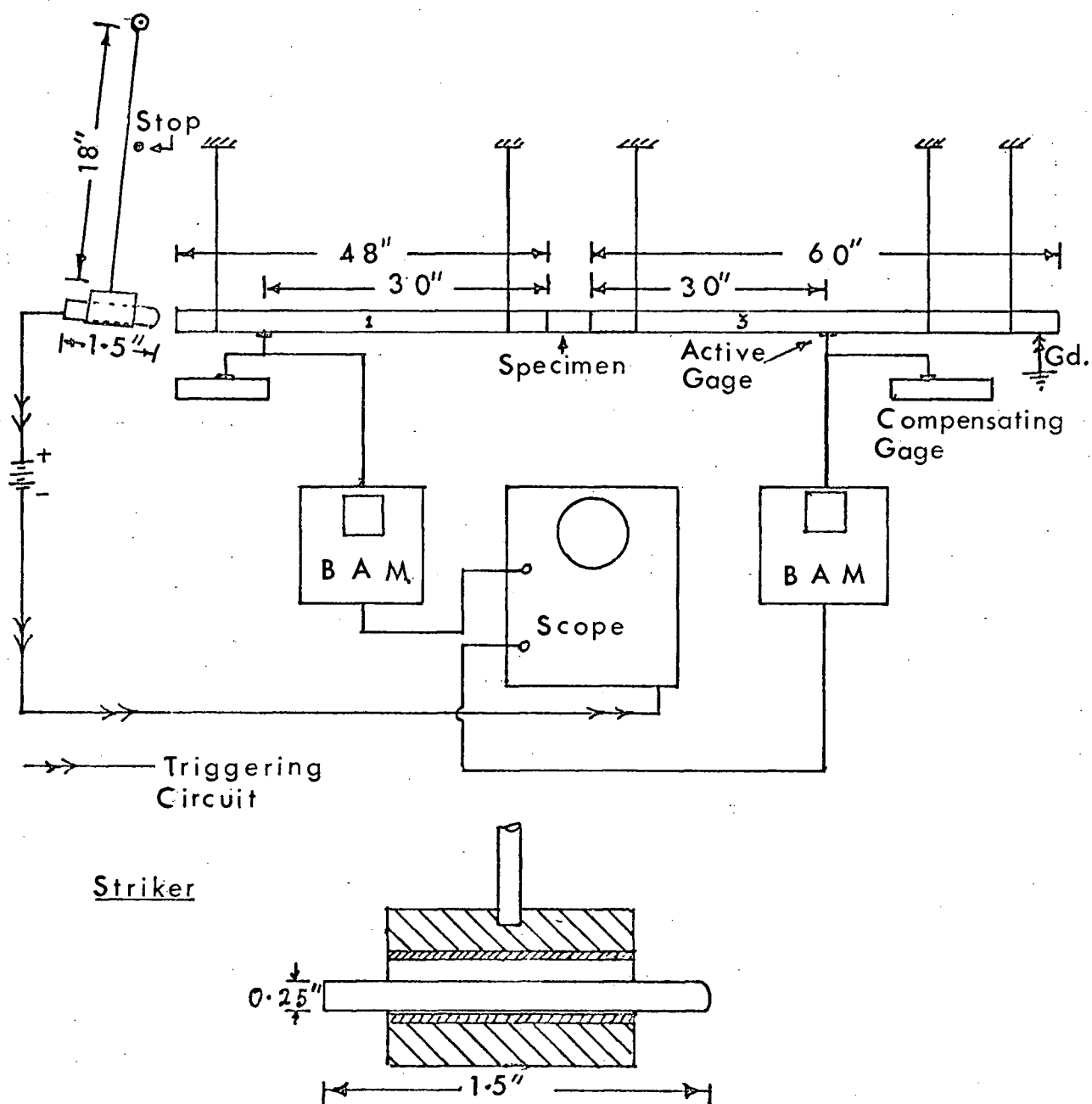
Figure 5.1.1   Schematic Diagram of Experimental Apparatus

from the free end and on bar 3, 30 in. away from the free end.
Two compensating gages were mounted on two different bars of
steel for temperature compensation.

The output from each of the half bridges, consisting
of one active and one compensating gage, was fed into separate
Bridge Amplifier Meters (BAM). The amplified output from the
BAM was observed and recorded on an oscilloscope. These
strain-time relationships were photographed (Figure 6.2.1) to
obtain a final record.

5.2   Details of Experimental Apparatus

5.2.1   Triggering Circuit:

By proper adjustment of the level switch, the oscillo-
scope can be triggered when an electrical pulse of more than
2 volts amplitude is applied to the external triggering terminals
of the scope. The triggering circuit has been shown in
Figure 5.1.1. A 12V pulse, produced by the contact of the
striker bar and bar 1, was employed to trigger the scope.

5.2.2   Strain Gage Locations:

The strain gages were mounted on the bars more than half
the length of the incident pulse away from the ends,

   i) to avoid any interference of the incident and trans-
      mitted pulses with the reflected pulses from the ends.
  ii) to avoid any localized three-dimensional effects at
      the ends.
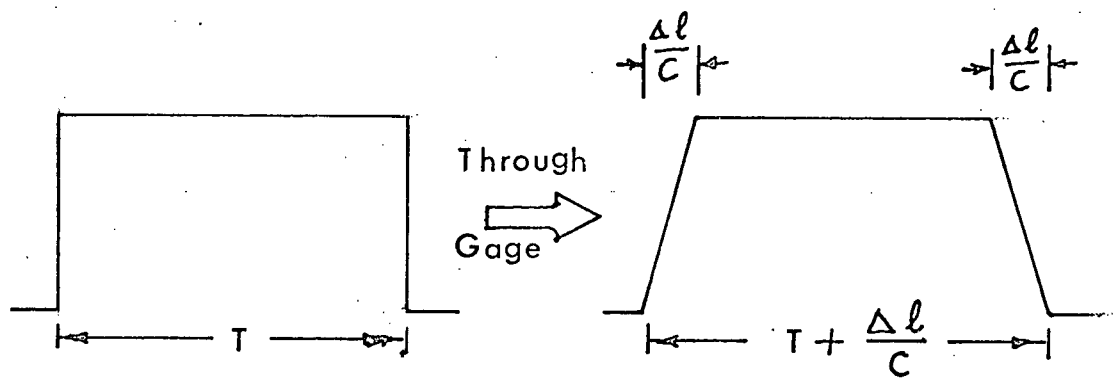
Figure 5.2.1 Error in Measuring Dynamic Strain with Strain Gages

5.2.3 Size of Strain Gages:

Some error [10] results when a strain gage is used to measure a strain pulse, due to the fact that a strain gage measures an average strain over its length Δl, rather than strain at a point. This effect is illustrated in Figure 5.2.1. A gage length of 0.25 in. was chosen. Since the wave length of highest frequency (20,000 cps) of interest is 10 in., the ratio of gage length to wave length (1/40) was quite low. Therefore the error in measuring instantaneous strain at a point was negligible.

5.2.4 Diameter of Bars:

Kolsky [11] has shown that the error in the determination of strain using one-dimensional wave propagation theory is proportional to a^2/λ^2 (where a is the diameter of the bar and λ is the wave length of strain wave). Since the shortest wavelength of interest in the steel bar is 10 in. (for 20,000 cps), the error involved is less than 1% for 0.25 in. diameter steel bar, and hence three dimensional effects, such as letral inertia, are negligible in the present circumstances.

5.2.5 Selection of Striker:

The highest frequency of interest was chosen as 20,000 cps. From Figure 4.2.1 which shows the modulus of the Fourier transform of a half sine wave, we have concluded that the amplitude for $\omega > 2.5p$ is less than 20% of the maximum amplitude at zero frequency. Therefore in order that the pulse contain significant components up to a frequency of 20,000 cps, it is necessary that

$$2.5p > 2\pi \times 20,000$$

where $p = \pi/T$ and the pulse duration is T, so

$$T < (2.5/2 \times 20,000) \quad \text{sec.}$$

Thus a pulse duration of less than 62.5 micro-sec is required. Davies and Hunter [6] have mentioned that in general mechanical systems are used for experiments in which load is applied in times of order of milliseconds or greater, while for pulses of microsecond duration, explosives are used. However, in the case of loading by explosive charges, the intensity of stress is very high ($>10^3$psi) and there is little control on the form of the pulse. Therefore a pendulum striker was chosen to produce a stress pulse, for there is greater control on reproducibility of the pulse form and the stresses involved are of the order of 100 psi.

A number of theories have been postulated and experiments conducted regarding the duration of a pulse produced by the impact between the bodies of different geometries, and these have been reviewed in Chapter 3. It was not feasible to achieve the ideal conditions of the theories in present work. However, different geometrical configurations, of the striker were investigated experimentally, and the time duration of the pulses recorded have been tabulated in Table 5.2.A.
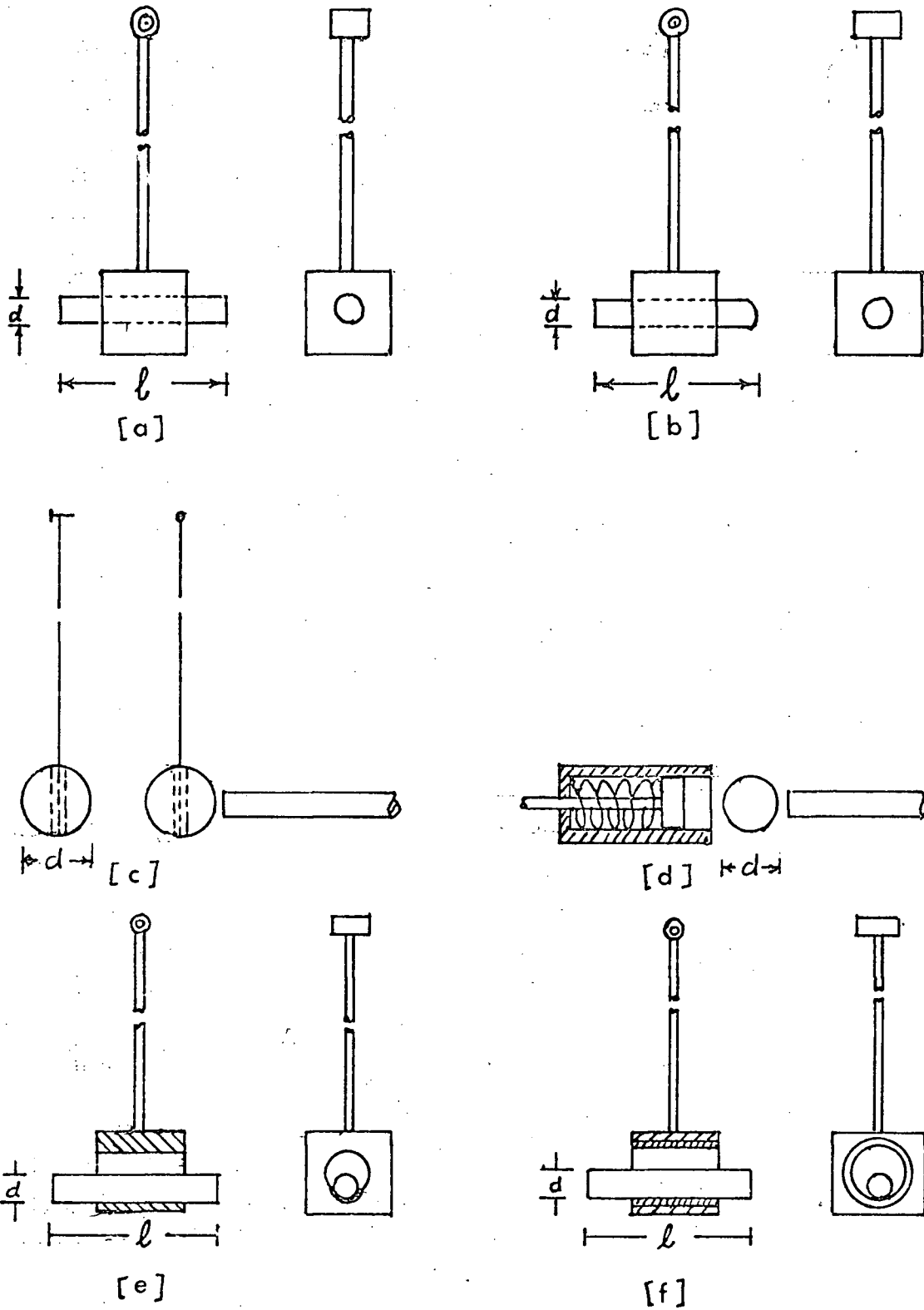
Figure 5.2.2   Striking Arrangements

Configeration 1:-

A flat-headed bar of length 1 was rigidly mounted at the end of the pendulum arm (Figure 5.2.2a).

Configuration 2:-

This configuration was similar to 1 except the striking head of the bar was rounded (Figure 5.2.2b).

Configuration 3:-

A ball bearing suspended by a heavy wire was used to strike the free end of the bar 1 (Figure 5.2.2c).

Configuration 4:-

A ball-bearing of diameter d was shot by a spring loaded shot gun, to achieve a free impact between the ball and the bar. (Figure 5.2.2d).

Configuration 5:-

This arrangement was used to achieve impact between two free bars. The striker bar rested in a semi-circular slot in the pendulum (Figure 5.2.2e).

Configuration 6:-

This arrangement was similar to 5 except that the slot was removed and the striker bar was free to slide in a smooth bronze bushing (Figure 5.2.2f).

TABLE 5.2.A

RESULTS OF STRIKER BAR STUDIES

s. No.	config- uration	l in.	d in.	Striker Geometry	Material	Time μ Sec	Remarks
1	1	3	1/2	▭ ◯	Steel	⩾ 300	S. No.1 through 5 gave results
2	1	3	3/8	-do-	-do-	150	with poor reproducibility
3	1	3	1/4	-do-	-do-	100	Pulse duration was increased
4	1	3	3/16	-do-	-do-	125	by increasing impact velocity.
5	1	3	1/4	-do-	Alumimimum	125	
6	1	1.5	1/4	-do-	Steel	125	
7	1	1.5	3/16	-do-	-do-	125	
8	2	3	1/4	▢ ◯	-do-	125	
9	2	1.5	1/4	-do-	-do-	>100	Imperfect impacts.
10	3	-	9/16	◯ ◯	Ball Bearing	80-150	Higher impact velocity gave a
11	3	-	3/4	-do-	-do-	100-200	smaller pulse duration.
12	4	-	9/16	-do-	-do-	-	Nothing could be recorded due to rattling of the ball.
13	5	3	3/8	▭ ◯	Steel	150-200	
14	5	3	1/4	-do-	-do-	-do-	
15	5	3	3/16	-do-	Steel	-do-	
16	5	1.5	3/8	-do-	-do-	-do-	
17	5	1.5	1/4	-do-	-do-	-do-	
18	5	1.5	3/8	▭ ◯	-do-	-do-	
19	5	1.5	1/4	-do-	-do-	-do-	

Table 5.2.A (continued)

S. No.	config- uration	l in.	d in.	Striker Geometry	Material	Time μ Sec	Remarks
20	6	1.5	1/4	-do-	Wood	130	
21	6	1.5	1/4	▭ ○	Steel	80-110	Poor reproducibility.
22	6	1.5	3/8	-do-	-do-	-do-	-do-
23	6	1.5	1/4	▭ ○	-do-	~ 100	Good results.
24	6	1	1/4	-do-	-do-	~ 100	

As Table 5.2.A shows, in the twenty-four different arrangements tried, it was not possible to produce a pulse of smaller duration than 62 μ sec. The best results were obtained for configuration 6 with a 1.5 in. long round-headed steel bar of 0.25 in. diameter sliding in the bronze bushing.

5.2.6 Selection of Specimens:

It was shown in Chapter 4 that the greater the difference in the impedance (z=E/c) in the two contiguous materials, the less the energy transmitted. Hence the following were the criteria in selection of a specimen:

i) The ratio (λ_1) of the difference and sum of the impedances of steel and the material of the specimen should be large.

ii) The material should be strong enough to support enough load so that it may be used in buildings and structures.

iii) Some materials exhibit the property of internal friction, which, in many instances, can be treated by linear viscoelasticity. The energy of a stress wave is dissipated while propagating through such material.

iv) The length of the specimen has been chosen (a/h<<25) to eliminate the effects of radial and tangential friction [6] but short enough to be used economically in applications.

Table 5.2.B shows approximate values of different relevant material properties

TABLE 5.2.B

MATERIAL PROPERTIES

Material	$EX10^{-6}$ psi	$CX10^{-4}$ in/sec.	Z psi-sec./in.	$\lvert 1-\lambda_1 \rvert$
Aluminum	10	6	170	.94
Steel	30	20	150	1
Copper	15.6	4	390	.56
Lead	2.35	4.34	54	.5
Nylon	.18-.45	5.36	3.3-8.3	.07

The materials tested were pure lead, 3% antimonial lead, 7% antimonial lead and nylon. Nylon was chosen as a typical high polymer. All specimen were 0.25 in. in diameter, and 0.25 in., 0.50 in. and 0.75 in. in length. For these proportions criterion IV, listed was satisfied.

6. RESULTS AND DISCUSSION

The first part of this chapter deals with the performances of the system, and shows the extent to which the requirements are satisfied and what limitations were encountered. The second part deals with the checks on the observations and results.

6.1 Performance of the System and its Limitations

6.1.1 Duration of Pulse:

The system finally selected to produce the stress pulse gave a pulse of about 100 microseconds duration as against the required 62 microsecond or less. However, since the pulse produced was not a half sine wave, the Fourier Transform of the pulse covered frequencies, from zero to 20,000 cps as shown in Figure 6.1.1.

6.1.2 No Distortion of Pulse:

As shown in Figure 5.1.1, strain gages on bars 1 and 3 were mounted 30.0 in. away from the specimen. To check that there was no distortion of a pulse as it propagates in the steel transducer bars 1 and 3, experiments were carried out on a continuous 8 ft. steel bar (Figure 6.1.2). No distortion was found (Figure 6.1.3) for the propagation of a pulse over a distance of 120 in. It was possible to observe the wave over this distance by taking account of the reflected pulse. Therefore it can be concluded that the wave forms recorded by the strain gages on the transducer bars 1 and 3 give an accurate indication of the wave at the junctions with the specimen, bar 2.
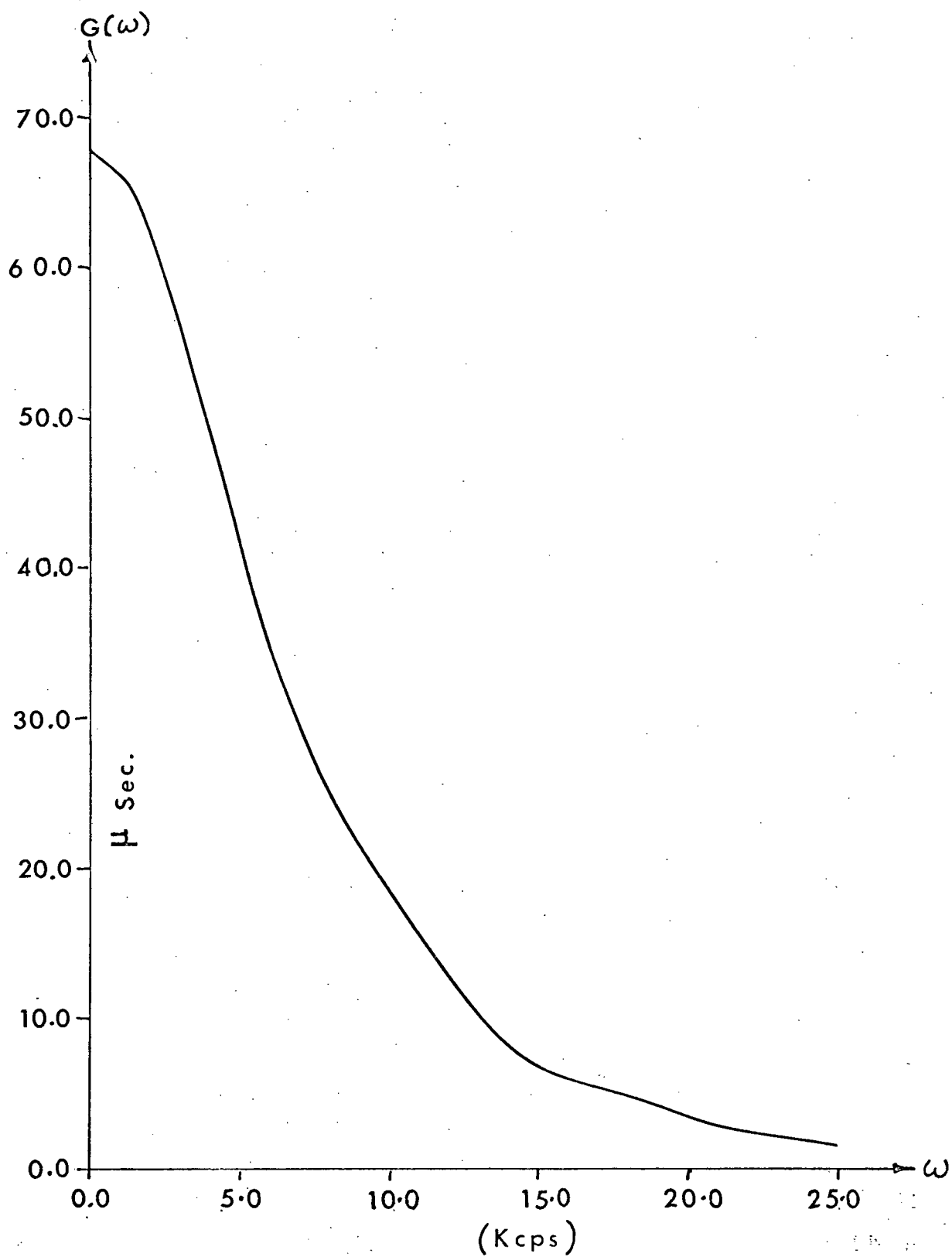
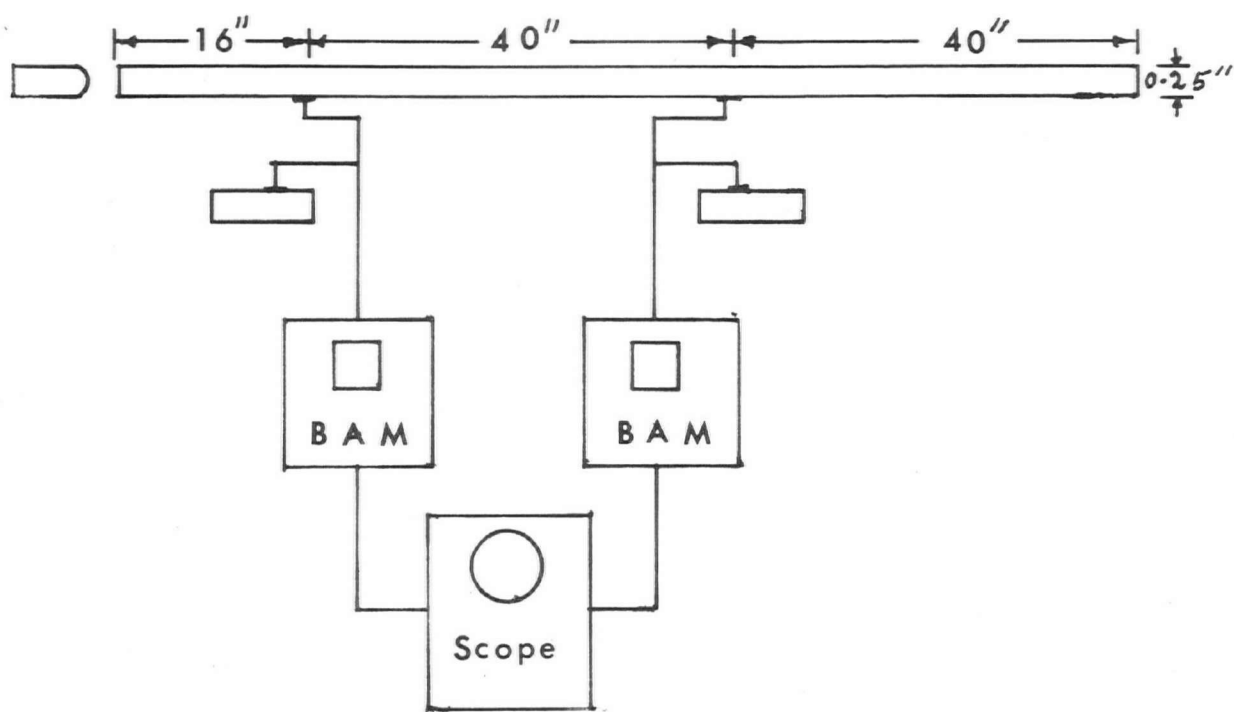Figure 6.1.1   Fourier Transform of Observed Pulse

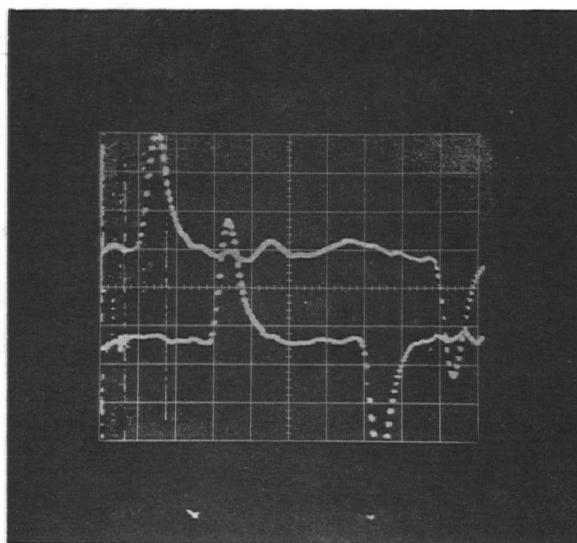Figure 6.1.2 Setup to Check Condition of No Distortion of Pulse

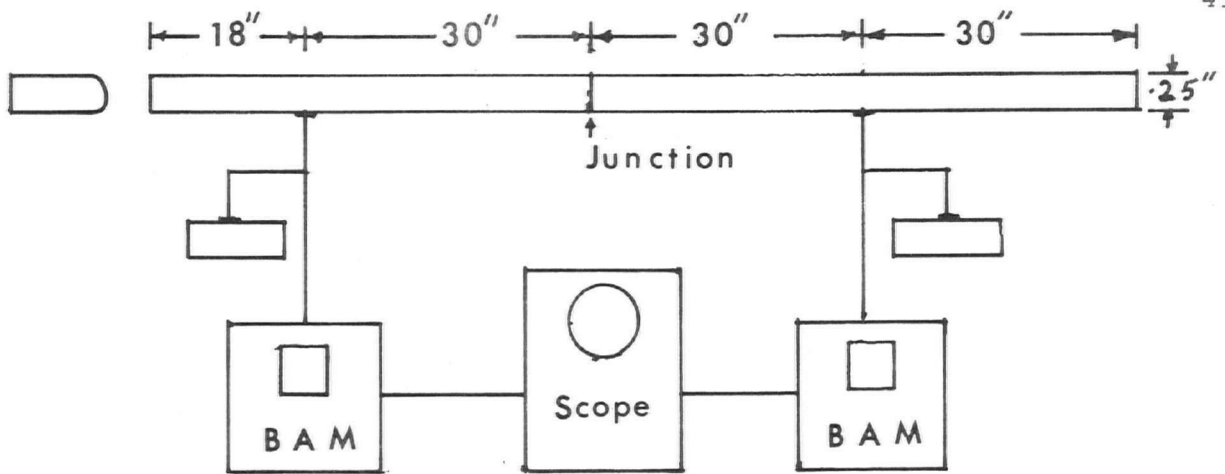Figure 6.1.3 Record Showing No Distortion of Pulse

Figure 6.1.4 Setup to Check Effect of Adhesive

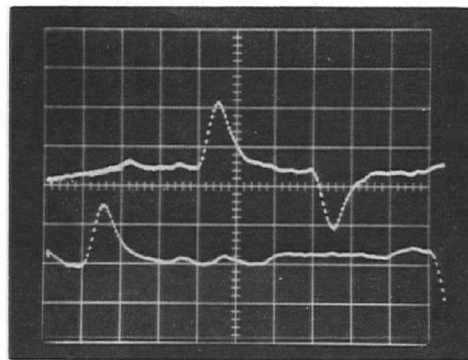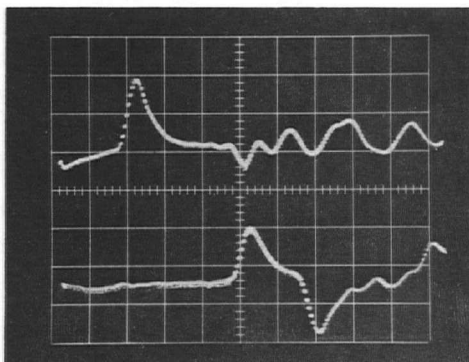Records to Show the Effect of Adhesives
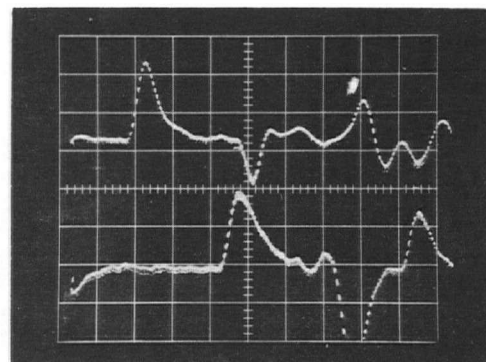

Figure 6.1.5 Paint

Figure 6.1.6 Grease

Figure 6.1.7 No Adhesive

6.1.3 Effect of Adhesive:

To hold the specimen in position, paint was used as
an adhesive. To make sure that the point does not cause any
reflection of the pulse, an experiment was conducted by join-
ing with paint the two steel bars of 0.25 in. diameter (Figure
6.1.4) and recording the pulse in each bar. The record (Figure
6.1.5) shows that there is no reflection of the pulse at the
joint. Figure 6.1.6 and Figure 6.1.7 were recorded for similar
experiments conducted by using grease at the joint and by
keeping the bar in contact just by applying slight pressure
(no adhesive used). Both Figure 6.1.6 and Figure 6.1.7 show
reflection of the pulse at the joint as compared to no reflec-
tion in case of Figure 6.1.5. The Fourier transforms for the
incident and transmitted pulses have been shown in Figure 6.1.8
for the case of two bars in Figure 6.1.4 joined together with
paint. This establishes that the presence of paint causes no
reflection or distortion at the juction.

Since the BAM had a constant gain up to 15,000 cps, and
since the modulus of the Fourier transform of the incident
pulse at 15,000 cps is less than 10% of the maximum amplitude
at zero frequency (Figure 6.1.1) the results were plotted up
to 15,000 cps only.

6.2 Checks on Observations and Results

A typical stress-time relationship record is shown in
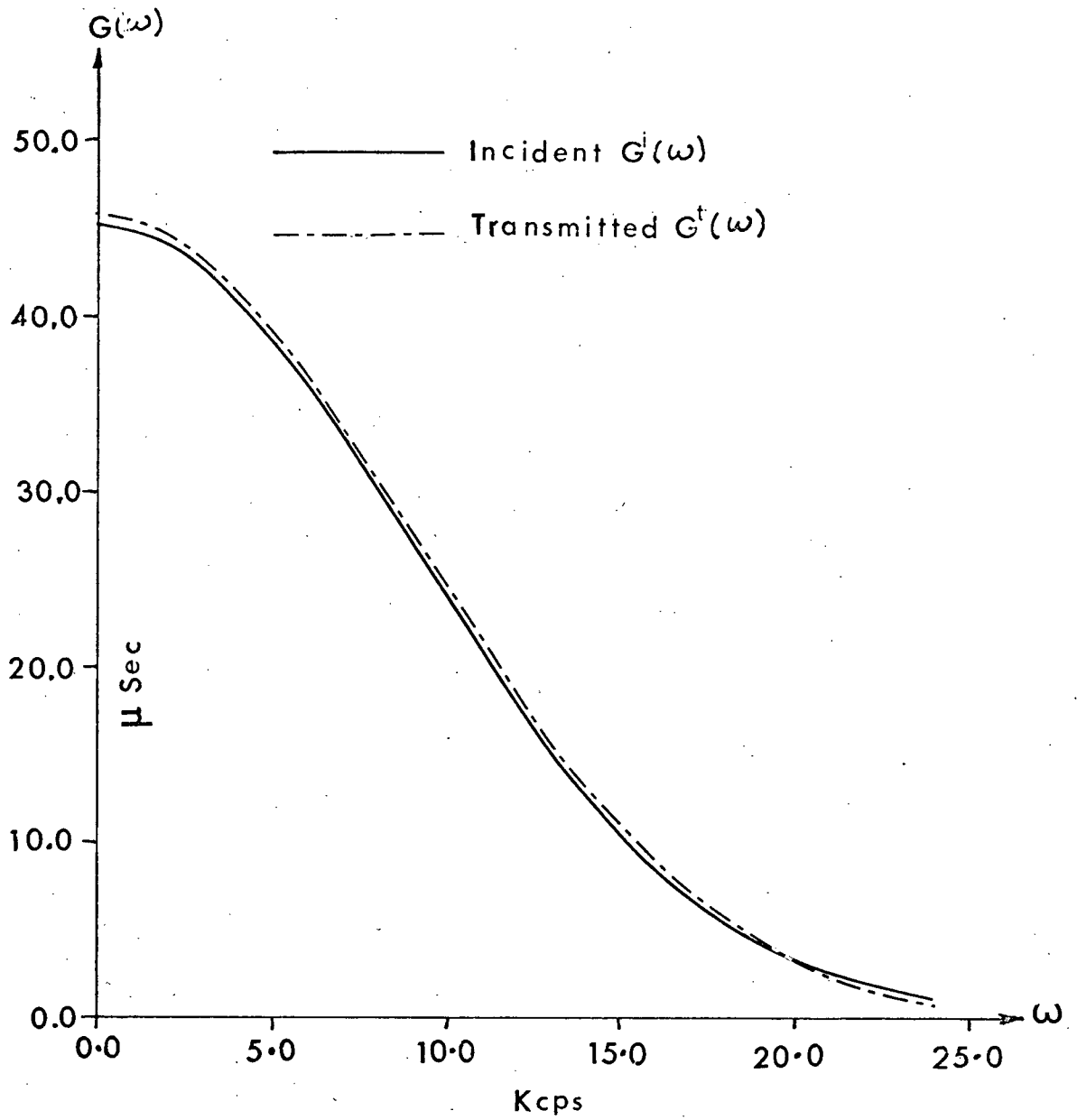Figure 6.2.1. The following checks and observations were made:

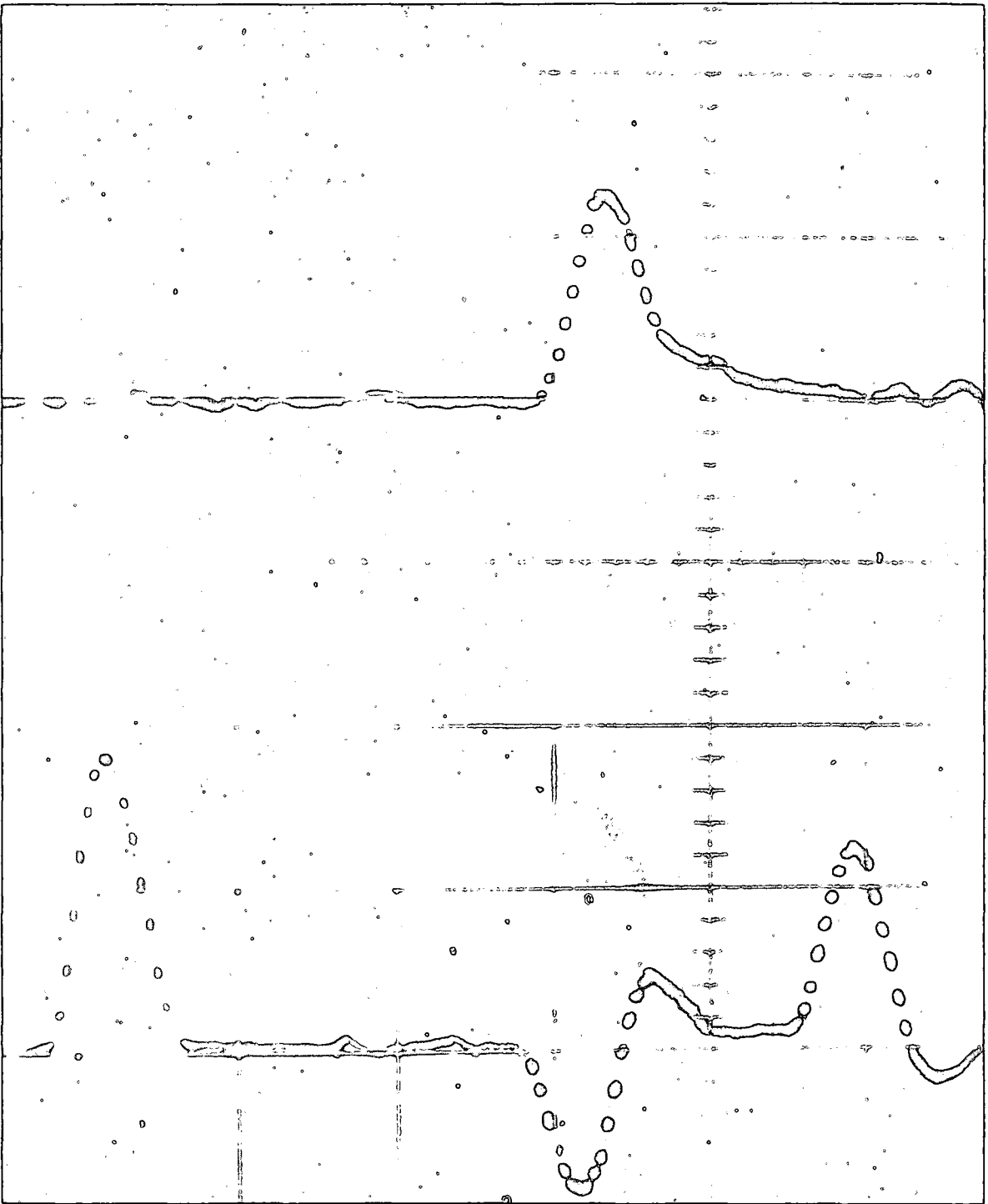Figure 6.1.8   Fourier Transform of Pulses Recorded for Paint

Figure 6.2.1 Stress-Time Relationship

i) The calculated velocity of sound in steel is about 20×10^4 in/sec ($c = \sqrt{E/\rho}$, $E = 30 \times 10^6$ psi $\rho = .282$ lb/in^3); therefore the transmitted and reflected pulses should commence 300 microsecond after the commencement of the incident pulse for a pair of strain gages mounted 30.0 in. away from the junctions. This checks with Figure 6.2.1.

ii) In the presence of a specimen, the transmitted pulse appeared attenuated (Figure 6.2.1) as compared to the incident pulse.

iii) Dispersion was observed in the transmitted and re-flected pulses (Figure 6.2.1) with respect to the incident pulse.

iv) The transmitted pulse was always observed to be com-pressive for a compressive incident pulse.

v) The reflected pulse was tensile initially and changed to compression.

All observations, ii through v, check with the simple theory developed in Chapter 4 for an elastic specimen, bar 2. The infinite duration of the transmitted and reflected pulses (found theoretically) could not be observed practically due to small amplitudes associated with the trailing part of the pulses.

The reflected pulse, being longer than 36.0 in., could not be isolated from its own reflection (figure 6.2.1) from the free end of the bar 1, which was 18 in. away (Figure 5.1.1) from the gage.

Figure 6.2.2 shows $G^i(\omega)$, $G^t(\omega)$ and $L(\omega)$ plotted against frequency; $G^i(\omega)$ and $G^t(\omega)$ are the moduli of the
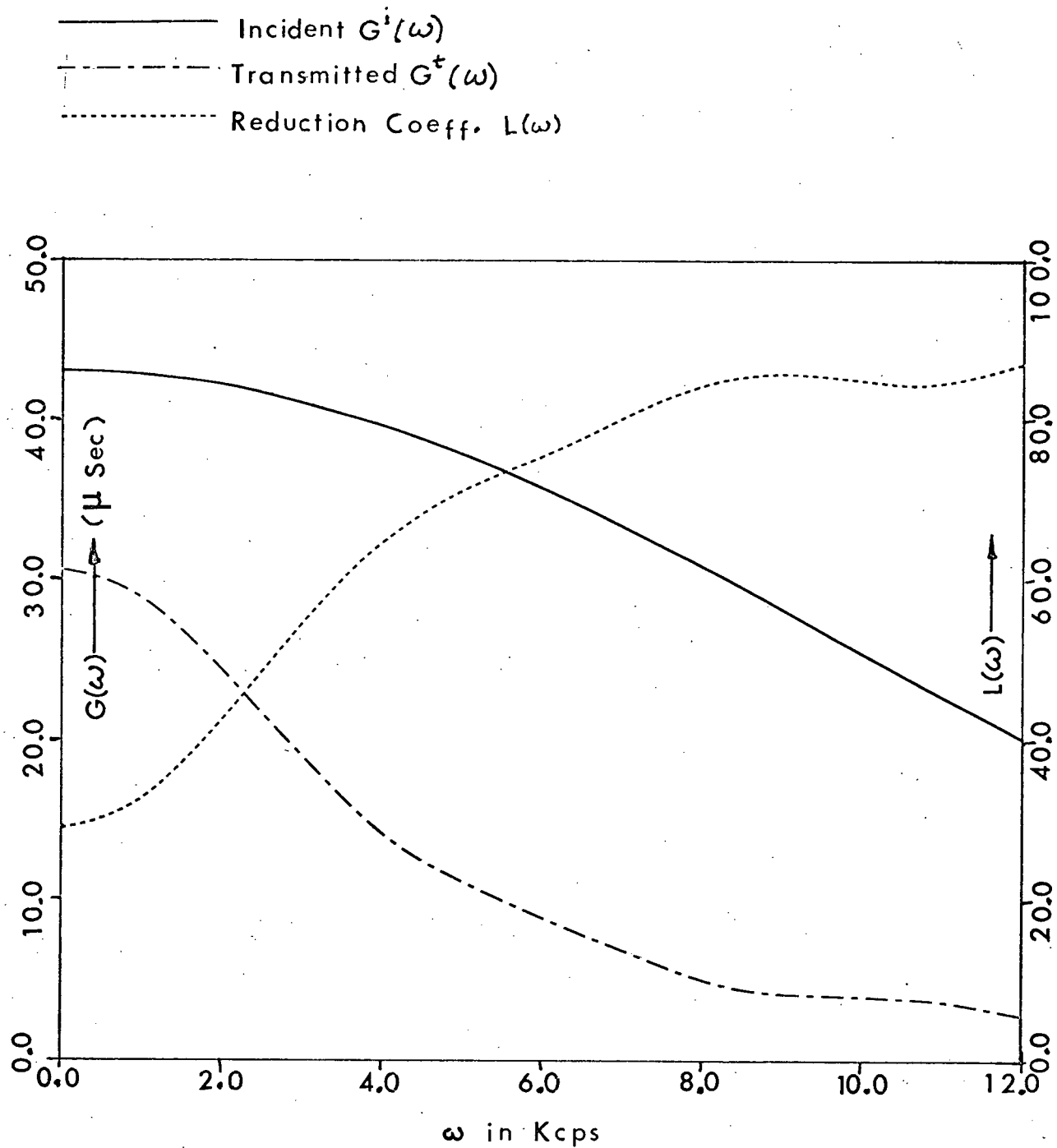
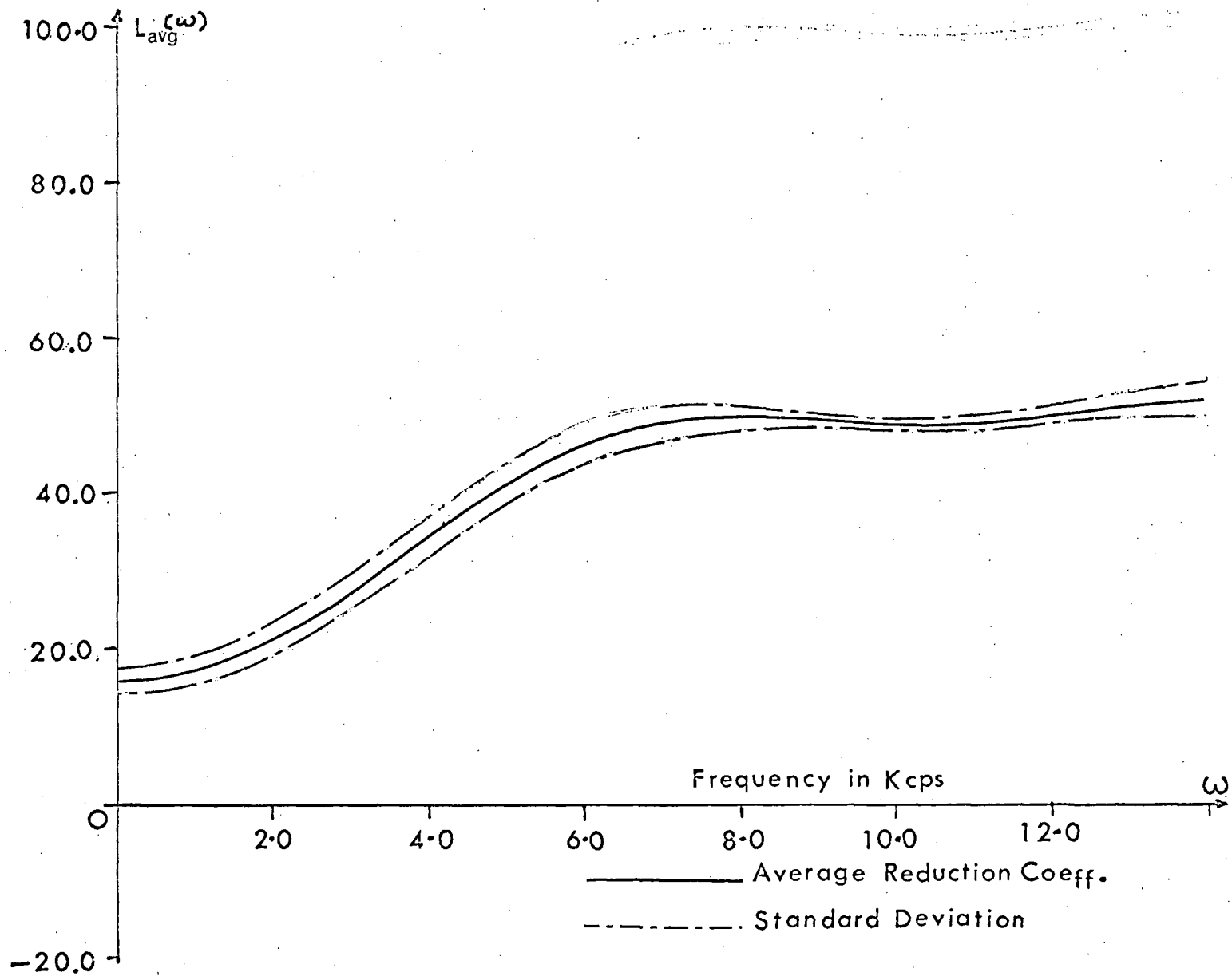Figure 6.2.2   Fourier Transforms and Reduction Coefficient

Figure 6.2.3   Average Reduction Coefficient for 0.75 in Lead

Fourier transforms of the incident and the transmitted pulses and $L(\omega)$, the reduction coefficient $(=[G^i(\omega)-G^t(\omega)]x100/G^i(\omega))$, is the percent reduction in amplitude. The final results presented, Figure 6.2.3, show $L_{avg}(\omega)$ (r.m.s. average) with standard deviation lines bounding it to give an indication of the scatter in the results.

Most of the results show that the reduction coefficient is not zero at zero frequency. This observation could not be accounted for by the simple theories developed in Chapter 4 for the case of elastic and linear viscoelastic specimens, since these theories predict that the reduction coefficient at zero frequency should be zero. This effect may be due to non-linear behaviour of the material.

Checks on the conservation of momentum could not be made accurately as the complete information about the reflected pulse was not available. However, approximate checks made on some photographs satisfied (4.3.5).

Some cases have shown a peculiar behaviour of a negative reduction coefficient for a range of small frequencies. Such behaviour is not in accord with the linear theories developed in Chapter 4. One such case is shown in Figure 6.2.4. The area and hence the momentum of the transmitted pulse are greater than the area and the momentum of the incident pulse. Also since the area of the compressive part of the reflected pulse is greater (in absolute value) than the area of the tensile part of the reflected pulse, the reflected pulse has positive momentum. The amplitude of the Fourier transform at zero
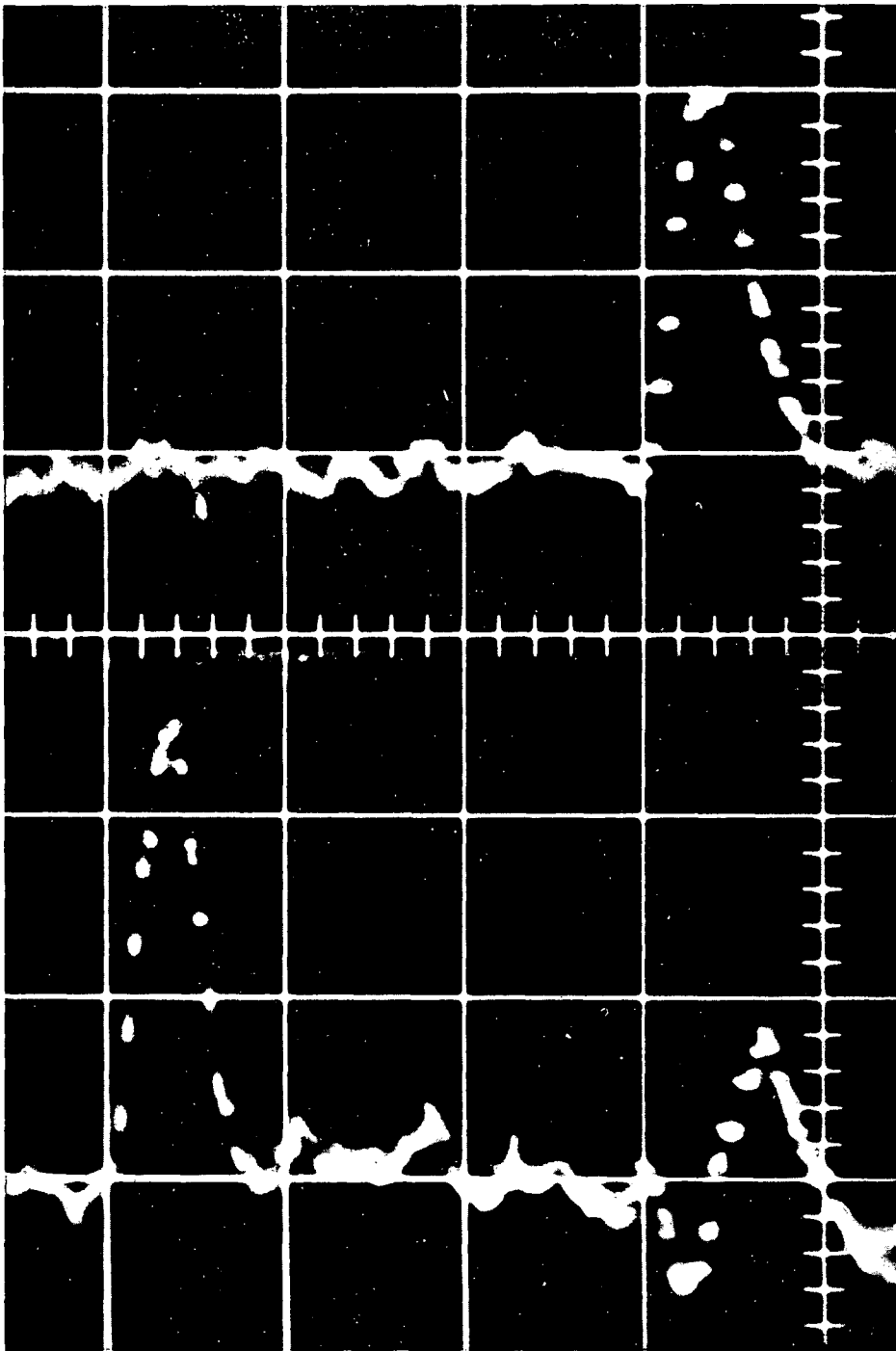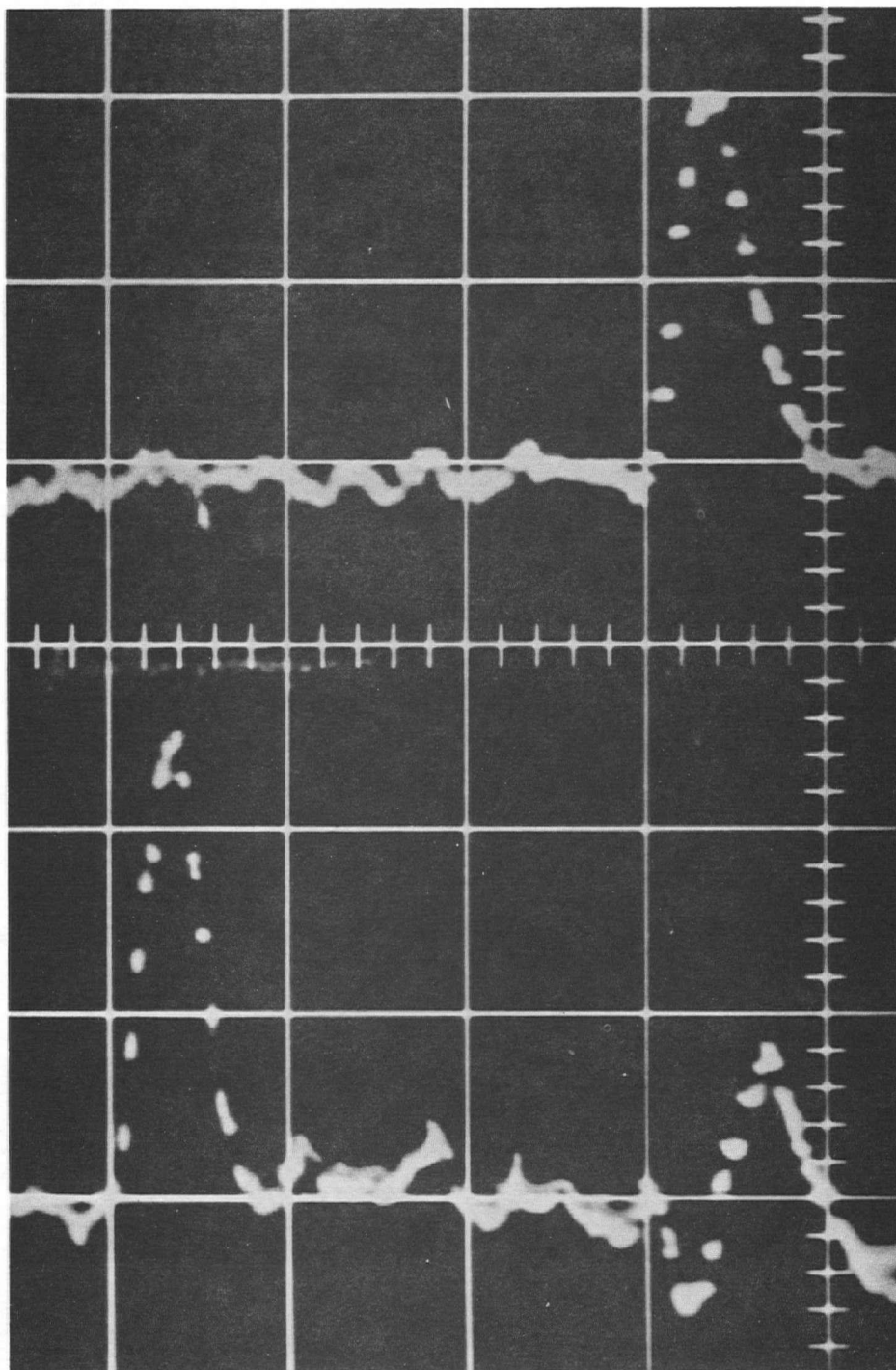
Figure 6.2.4   Stress Strain Relationship

Figure 6.2.4   Stress Strain Relationship

frequency is proportional to the momentum of the pulse. Hence a negative reduction coefficient is related to the distribution of momentum discussed above.

The energy carried in the incident pulse is proportional to

$$\int_{-\infty}^{\infty} [\sigma_1{}^i(x,t)|_{x<0}]^2 \, dt \ .$$

By calculating the corresponding integral for the transmitted pulse in bar 3, it was found that there was a reduction in the energy transmitted, even for this case of a negative reduction coefficient.

The results can be considered useful only up to 12,000 cps as the deviation for $\omega > 12,000$ cps are rather high. The higher frequency components in the Fourier transform arise due to sudden changes in slopes which could not be defined accurately with the photographs taken in the present work. This may be the reason for larger deviations for $\omega > 12,000$ cps.

7. CONCLUSION AND REMARKS

It has been found that the approach adopted in the present work is a very good method for studying the frequency response of different materials. The impact of the striker bar produces a pulse which is of suitably small amplitude (~250 psi) and contains frequencies up to 15,000 cps. Explosive charges, on the other hand, produce high amplitude pulses and the waveform is more difficult to reproduce. It is very difficult to produce a stress pulse with the duration of microsecond range by mechanical devices.

A stress pulse (within the elastic limit) propagating through a steel bar does not distort. The use of paint to hold the specimen between the two steel transducer bars is an excellent technique which does not destroy the surfaces in contact.

The following points, established theoretically for the cases of elastic specimens, bar 2, were verified experimentally for the specimens used in the present research:

i) The transmitted pulse has the same sign as the incident pulse; i.e. if the incident pulse was compressive, the transmitted pulse was also found to be compressive.

ii) The transmitted pulse was found to be attenuated and dispersed as compared to the incident pulse.

iii) It was also verified that the reflected pulse had both compressive and tensile parts.

iv) Energy transmitted to bar 3 was less than the energy in the incident pulse in bar 1.

As opposed to the results of simple linear theory, the momentum of the transmitted pulse was not found to be equal to the momentum of the incident pulse. This result may be attributed to nonlinear viscoelastic behaviour of the material of the specimen.

Results show that reduction coefficient is a function of frequency, and also of thickness and material of the specimen. In general the reduction coefficient increased with the following factors:

i) An increase in thickness of the specimen. This can be observed by comparison of the $L_{avg}(\omega)$ curves for the specimens of different lengths of the same material. A pulse propagating in a longer viscoelastic material is attenuated more than in a shorter one.

ii) An increase in the ratio of difference and sum of the impedances of the coupled materials. This can be observed by comparing $L_{avg}(\omega)$ curves for the specimens of the same length but of different materials.

iii) An increase in the viscous damping of the material. For pure lead, 3% and 7% autimonial lead, the value of quantity λ_1 is almost the same, but a comparison of $L_{avg}(\omega)$ curves for 0.75 in. long specimens of the three materials distinctly shows an increased reduction coefficient for pure lead, which has the highest viscous damping coefficient of all the three.

iv) An increase in frequency. Every $L_{avg}(\omega)$ curve shows an increase in the reduction coefficient with increasing frequency except a few which show a decrease for higher frequency.

8. SUGGESTIONS FOR FURTHER WORK

The following suggestions can be divided into two groups.

8.1 Improvements and Changes in the Present Experimental Setup

I. For higher sensitivity, higher voltage output is required (it is desirable to achieve a sensitivity of at least 10 psi/mv and preferably 1 psi/mv or less). The sensitivity can be increased in following ways:

(a) Using a four gage bridge;

(b) Employing an additional d.c. source in series with the BAM, depending on the power restriction of the gages.

(c) Using a BAM with a higher amplification factor or a separate amplifier to amplify output from the BAM.

II. A band-pass filter (80 cps to 40,000 cps) may be used to eliminate any 60 Hz pick-up and high frequency noise.

III. To get a better description of the pulse, the time scale of the scope should be enlarged. This can be accomplished by using the triggering circuit shown in Appendix C, Figure C.1 and using the mechanical system shown in Figure 8.1.1. This will give a stress-time relationship hypothetically constructed in Figure 8.1.2.

IV. It would be easier to mount a speciment on a 0.5 in. diameter bar.

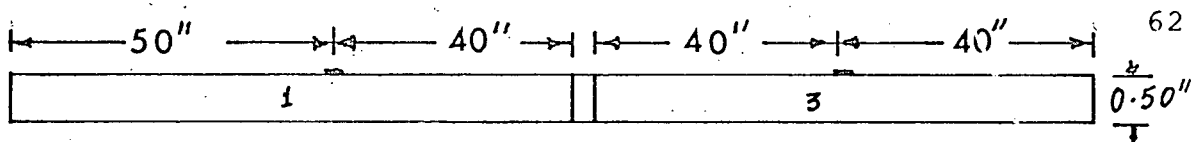V. Laminated specimens can be tried as they are being
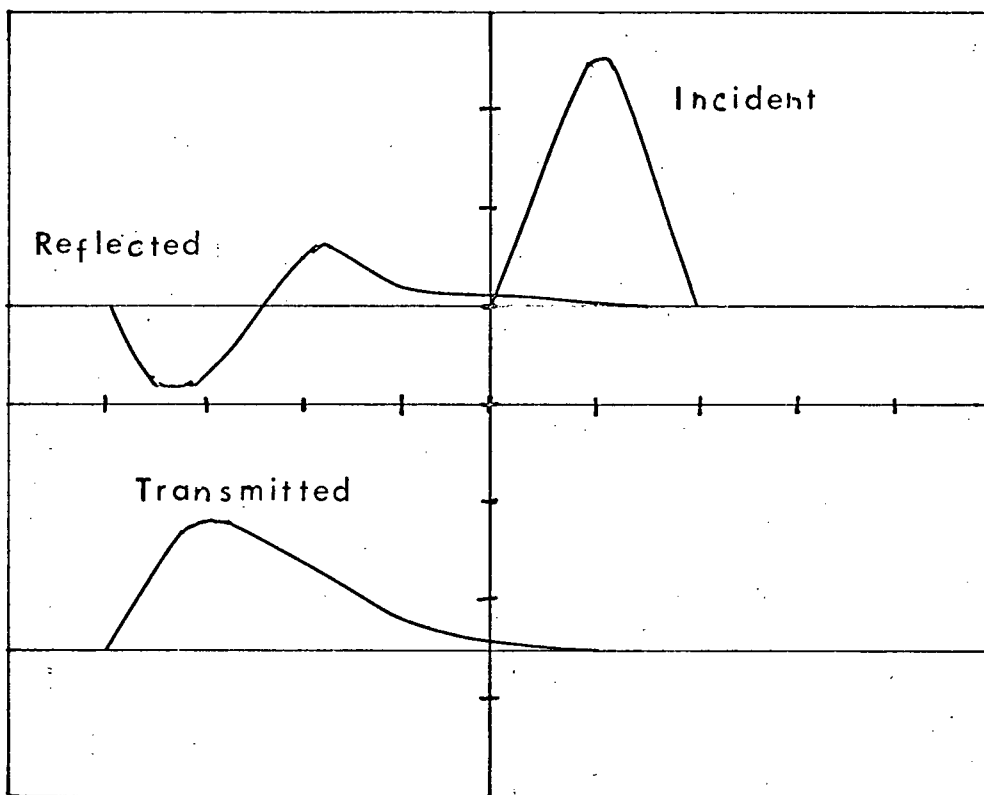
Figure 8.1.1 Suggested Mechanical System

Figure 8.1.2 Hypothetical Stress-Time Relationship

used in the foundations of buildings.

8.2 Suggestions for Further Analysis

Further analysis has been suggested which could be carried out using the data obtained from the setup suggested.

I. It may be shown for each stress-time relationship that:

$$\int_o^\infty \sigma_1{}^i(t)\,dt = -\int_o^\infty \sigma_1{}^r(t)\,dt + \int_o^\infty \sigma_2{}^t(t)\,dt\ .$$

II. Depending on the results obtained for each specimen, a viscoelastic model may be appropriate to interpret the results.

III. $E = E(\omega)$ and $c = c(\omega)$ can be computed numerically from (4.1.41) by an iterative technique.

BIBLIOGRAPHY

1. Kolsky, H. "International Symposium on Stress Wave Prop-
    agation in Materials," Norman Davids (editor), Interscience
    Publishers, Inc., New York.

2. Timoshenko, S. "Theory of Elasticity," (1st Edition),
    McGraw Hill, (1934), pp. 387-389.

3. Hertz, H* "Uber Die Beruhrung Ferter Elastischer Korper,"
    J. Reine Angew. Math., Vol. 92 (1881), p. 156. Reprinted
    in English in Hertz Miscellaneous Papers, London, MacMillan.

4. Prowse, W.A* "The Development of Pressure Waves During
    the Longitudinal Impact of Bars," Philosophical Magazine,
    Vol. 22 (1936), pp. 209-39.

5. Hopkinson, B* "A Method of Measuring Pressure Produced
    in the Detonation of High Explosives or by Impact of
    Bullets," Philosophical Transactions of Royal Society of
    London, Series A, Vol. 213, p. 411.

6. Davies, E.D.H. and Hunter, S.C. "The Dynamic Compression
    Testing of Solids by Method of the Split Hopkinson Pres-
    sure Bar," Journal of Mechanics and Physics of Solids
    (1963), Vol.11, pp. 155-179.

7. Voltera, E. and Zachmanoglou, E.C. "Use of Resistence
    Strain Gages and Pizoelectric Gages," from "Dynamics of
    Vibration," Charles E. Merrill Books, Inc., (1965),
    p. 565.

8. "Current Practises in Isolating Buildings from Vibration
    with Lead Asbastos Pads," AlA, No. 39-D, Lead Industries
    Association, N.Y. (1969).

9. "Lead to Control Sound and Vibration," 9 Acoustical Treat-
    ment, Sound and Vibration, (1969), Lead Industries Assoc-
    iation, Inc., N.Y.

10. Taylor, D.A.W. "Time and Amplitude Errors in Measurement
    of Dynamic Strain Pulses by Resistance Strain Gages,"
    International Journal of Mechanical Sciences (1964).

11. Kolsky, H. and Douch, L.S. "Experimental Studies in Plastic
    Wave Propagation," Journal of Mechanics and Physics of
    Solids, (1962), Vol. 10, pp. 105-123.

    * From the book listed in [7].

12. Kolsky, H.** Proceedings of Physics Society (1949), B 62, p. 676.

13. Hill, R** "The Mathematical Theory of Plasticity," (1950), Clarendon Press, Oxford.

    ** From the paper listed in [6].

APPENDIX A

Test Procedure:-

The specimen was glued with paint between two steel
bars suspended by strings. The pendulum was released from a
certain angle and the striker bar was made to strike the free
end of bar 1. The impact of striker bar with bar 1 triggered
the scope. The stress-time relationships produced by the
oscilloscope beam were photographed. For each specimen,
about ten photographs were taken with a 35 mm Ashai Pentax
camera on a Plus X film. These were enlarged to give 1 in^2 on
the print for 1 cm^2 on the scope. The time axis on the print
was 0.1 m sec/in. The pulses were digitized by reading points
at 10 micro-sec. intervals.

The results obtained from such photographs were very
erratic since the quality of the photographs was very poor. To
improve the quality, the sensitivity of the BAM was increased
by additional d.c. voltage. A photograph thus obtained has
been shown in Figure 6.2.1.

APPENDIX B

Calculations:-

The incident and the transmitted pulses, described in
Appendix A and Figure 6.2.1, were normalized by dividing
the ordinates of the pulses by maximum stress in the incident
pulse. Thus $A(\omega)$, $B(\omega)$ and $G(\omega)$ were defined as follows for
computing the results:

$$A(\omega) = \int_{-\infty}^{\infty} \frac{\sigma(t)}{\sigma^i_{max}} \cos \omega t \, dt$$

$$B(\omega) = \int_{-\infty}^{\infty} \frac{\sigma(t)}{\sigma^i_{max}} \sin \omega t \, dt$$

$$G(\omega) = [A^2(\omega) + B^2(\omega)]^{1/2} .$$

$A(\omega)$ and $B(\omega)$ were computed by numerical integeration. To check
the numerical method adopted numerical and analytical results
were computed for a half sine wave of duration of 100 micro-
second on which the points were described at 10 microsecond
intervals. The maximum error was less than 1%, up to 20,000 cps.

The reduction coefficient $L(\omega)$ was calculated after
finding $G^i(\omega)$ and $G^t(\omega)$ for the incident and the transmitted
pulses respectively, where $L(\omega)$ is given by

$$L(\omega) = \frac{G^i(\omega) - G^t(\omega)}{G^i(\omega)} \times 100 .$$

The reduction coefficient $L(\omega)$ was plotted for eight to
ten stress-time relationship records for each specimen. A

larger scatter (more than 4%) of points was observed in certain cases particularly at frequencies lower than 4,000 cps and higher than 10,000 cps. The high frequency components arise from sudden changes in slope while low frequency components are due to small gradients in the pulse. Therefore the inaccuracy and error in the results at low and high frequencies are possibly related to the following points.

i) Since the points on the recorded pulses could not be read at smaller intervals than 10 microsecond on the horizontal time axes, these measurements are within an accuracy of ±5 microsecond. Such an error was generally encountered either at the leading or the trailing end of the pulse, where the slopes are quite steep. Thus this may give rise to error at higher frequencies.

ii) The pulses could only be read with an accuracy of ±5 psi. This represents an absolute error, and hence the percent error in $G^i(\omega)$, $G^t(\omega)$, and $L(\omega)$ due to this absolute error, is greatest at high frequencies where $G^i(\omega)$ and $G^t(\omega)$ are small.

iii) The transmitted pulse, as found theoretically, should extend to infinite time. However, due to the very small amplitude associated with the trailing part of the transmitted pulse, it is impractical to read the pulse after a certain finite time. The omitted trailing part of the transmitted pulse may have a finite area which contributes to the low frequency componants of the Fourier transform.

Therefore, four consistent $L(\omega)$ plots (out of 8-10 plots)

were chosen to obtain the curves for $L_{avg}(\omega)$ given by

$$L_{avg}(\omega) = \sqrt{\sum_{j=1}^{4} L_j^2(\omega)/4}$$

$L_{avg}(\omega)$ was plotted in the final results bounded by the standard deviation lines described as

$$\left[L_{avg}(\omega) \pm \sqrt{\sum_{j=1}^{4} \{L_{avg}(\omega) - L_j(\omega)\}^2/4} \right].$$

A typical $L_{avg}(\omega)$ bounded by the standard deviation lines is shown in Figure 6.2.3.
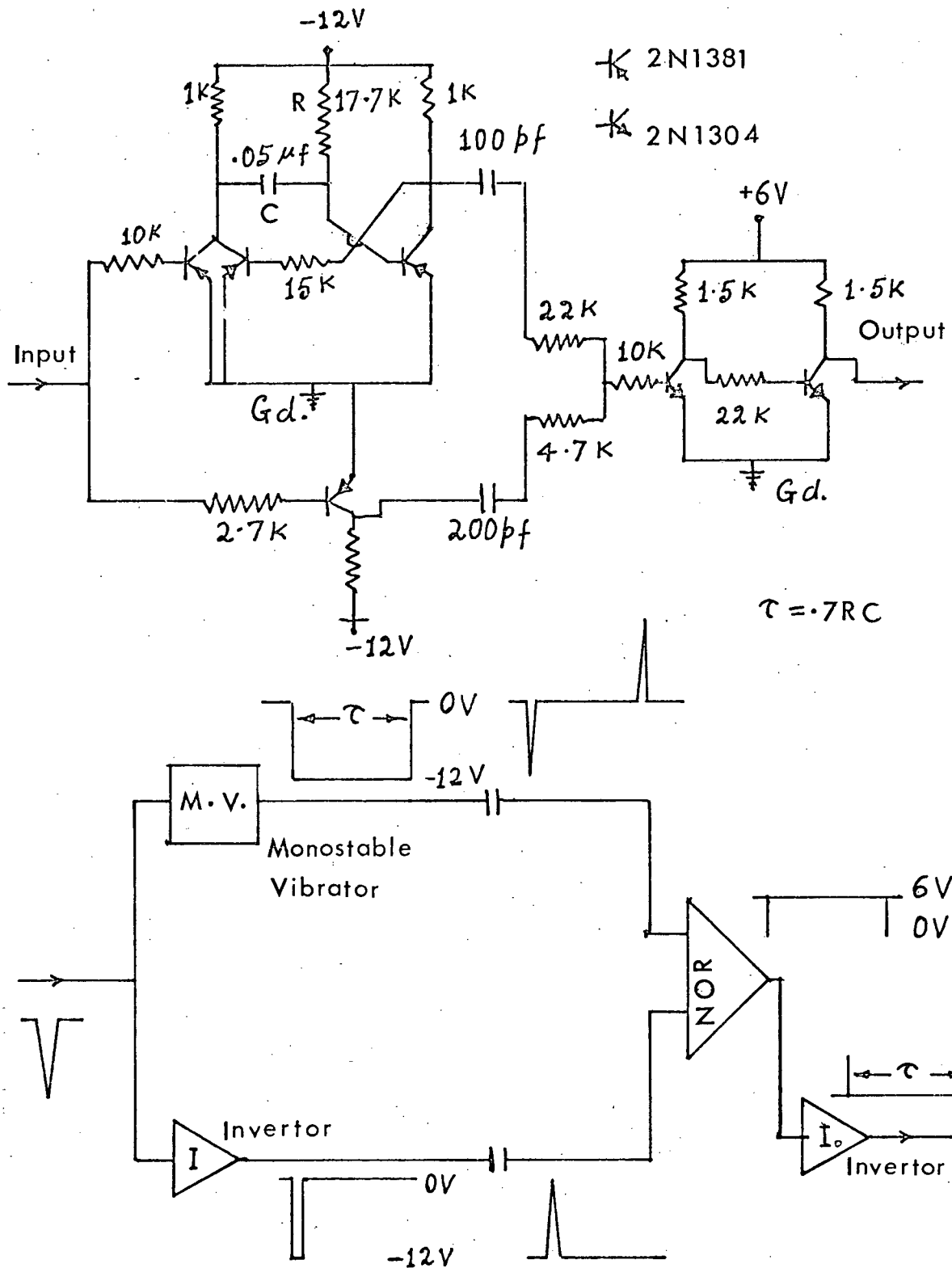
Figure C.1   Circuit for Two Triggering Pulses

APPENDIX C

Two triggering pulse-electronic circuit:

The Figure C.1 shows the circuit to obtain two trigger-
ing pulses from one electrical pulse produced by the contact
of the striker bar and anvil bar. The interval τ between the
two pulses is given by τ = .7RC.

For the circuit shown, the sweep time is 500 microsecond
and about 100 microsecond have been provided for reset time,
making τ = 600 microsecond.

Three or more triggering pulses can be generated by
adding one or more monostable vibrators to the circuit.

Elimination of invertor I would yield a delay circuit
giving a delay time τ = .7RC.

APPENDIX D

Additional Figures:

    i) Reduction Coefficient:

    The following figures show the average reduction coefficient ($L_{avg}(\omega)$) for twelve specimens which were tested.
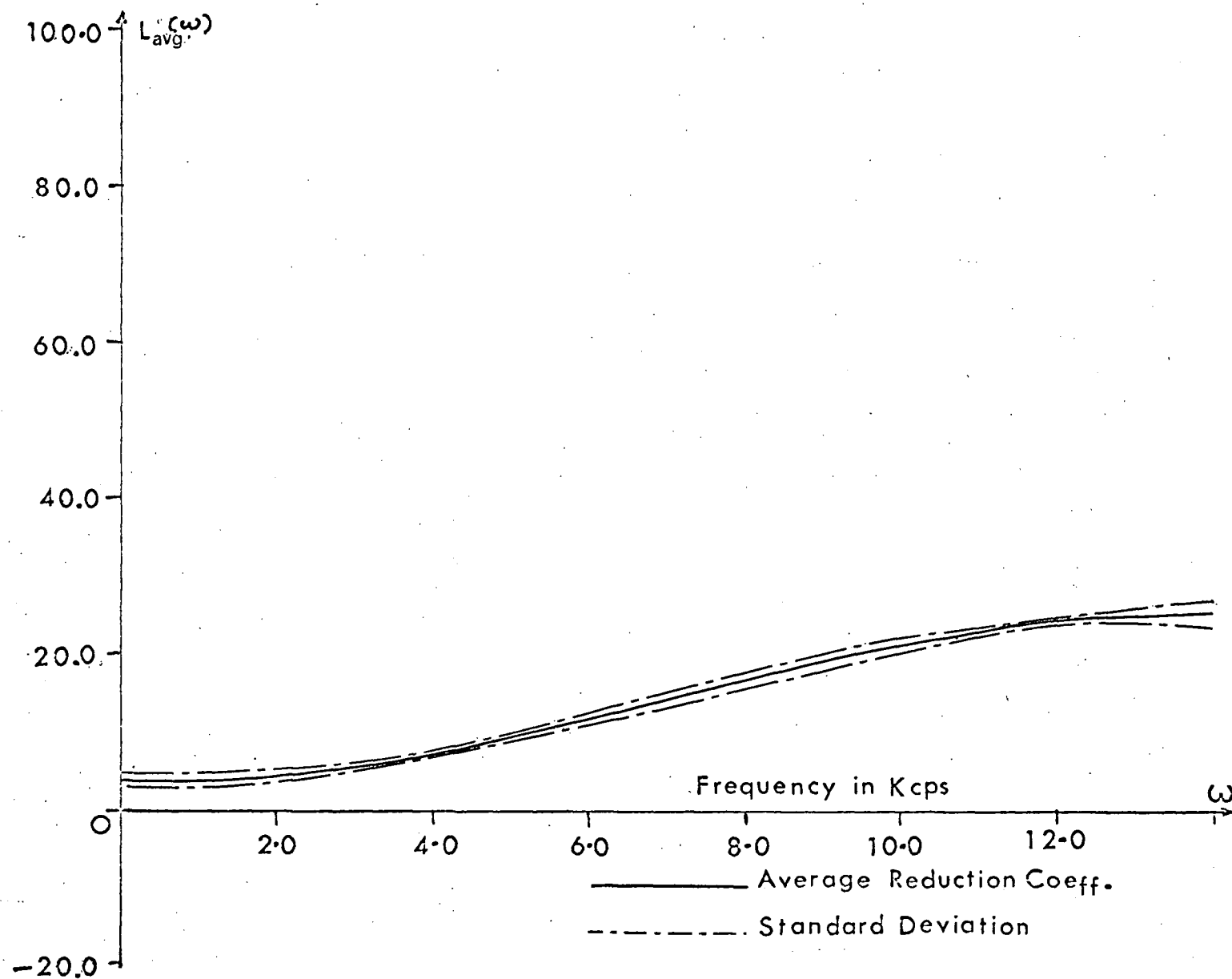
Figure D.1   Average Reduction Coefficient for 0.25 in long
7% Antimonial Lead
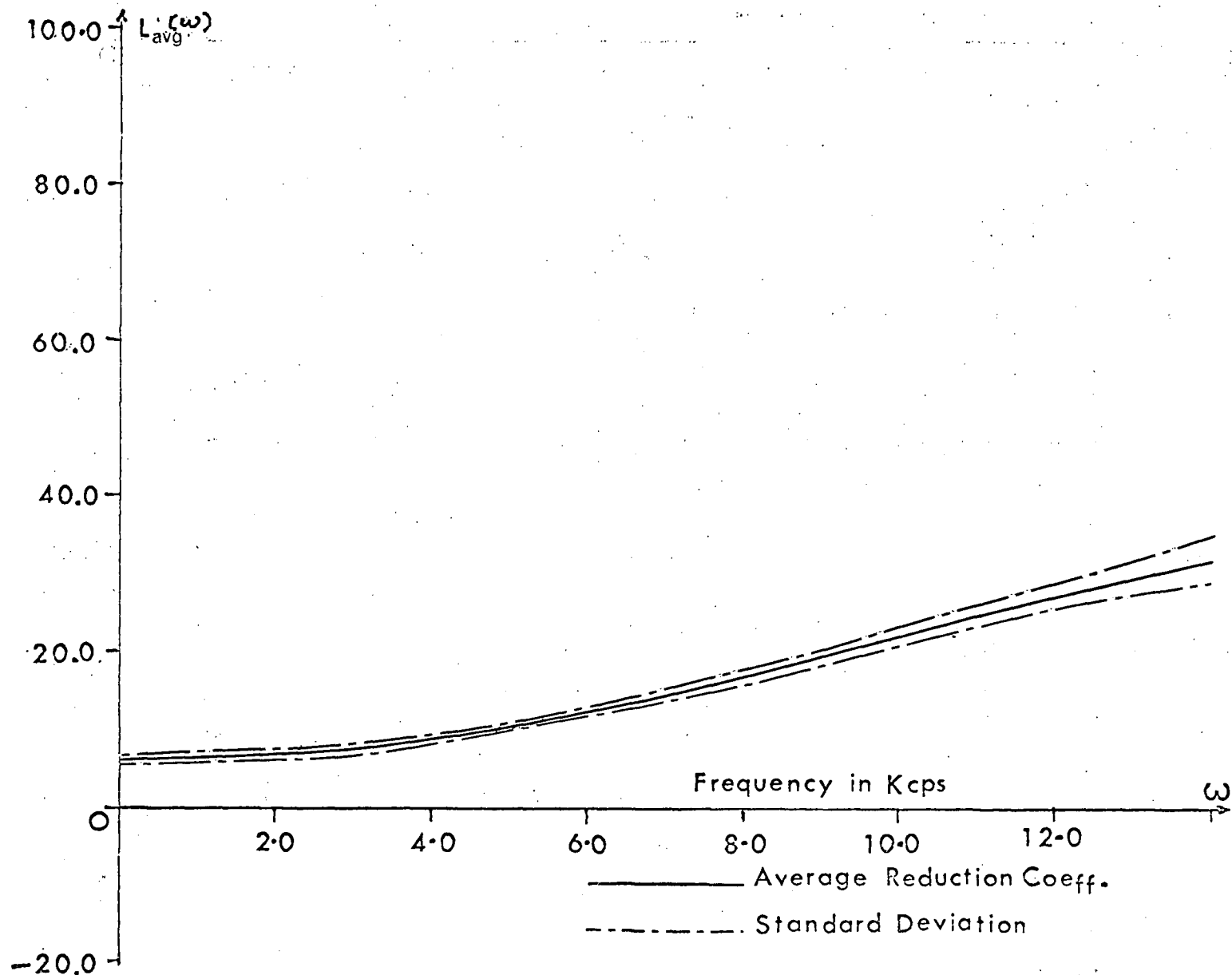
Figure D.2   Average Reduction Coefficient for 0.50 in long 7% Antimonial Lead
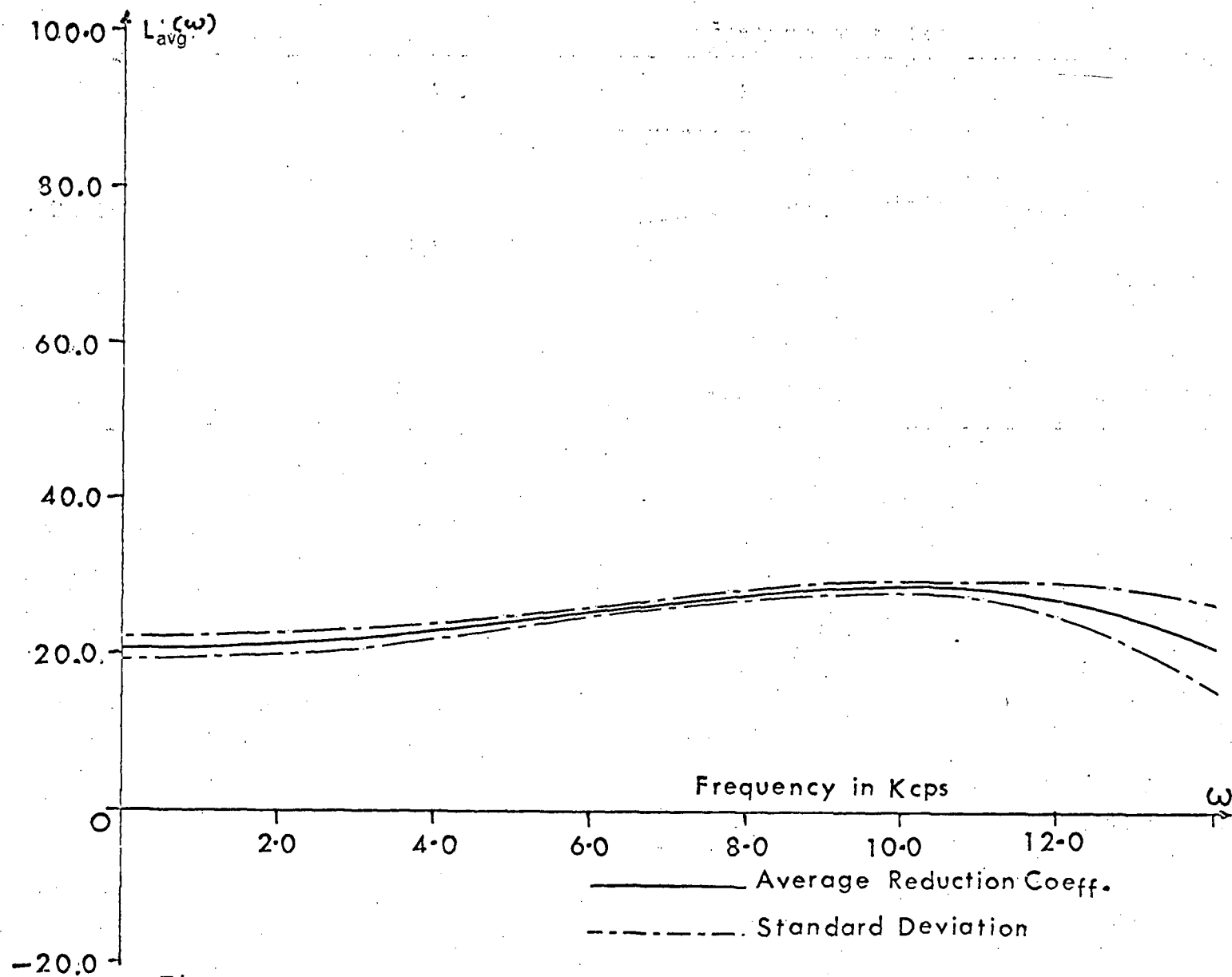
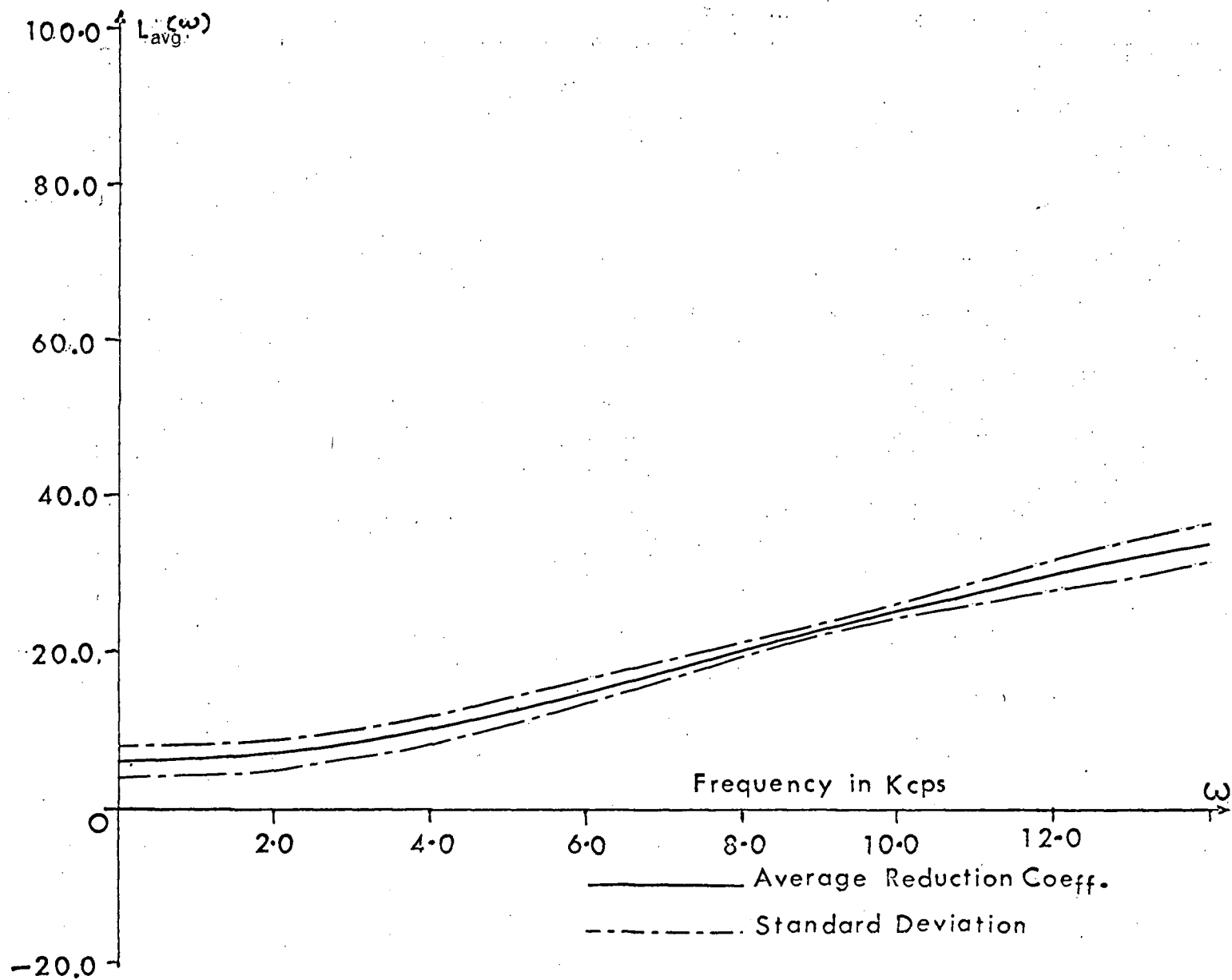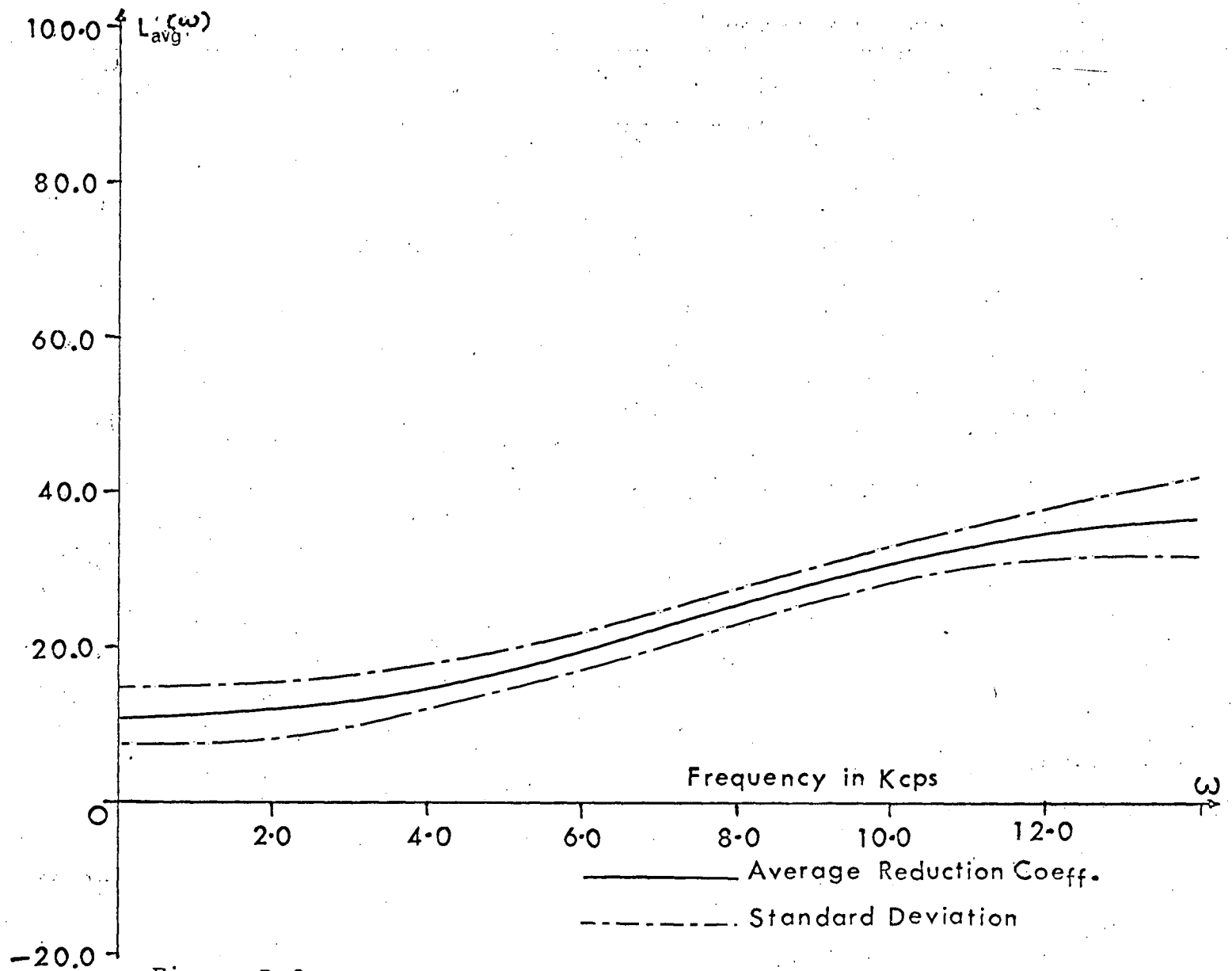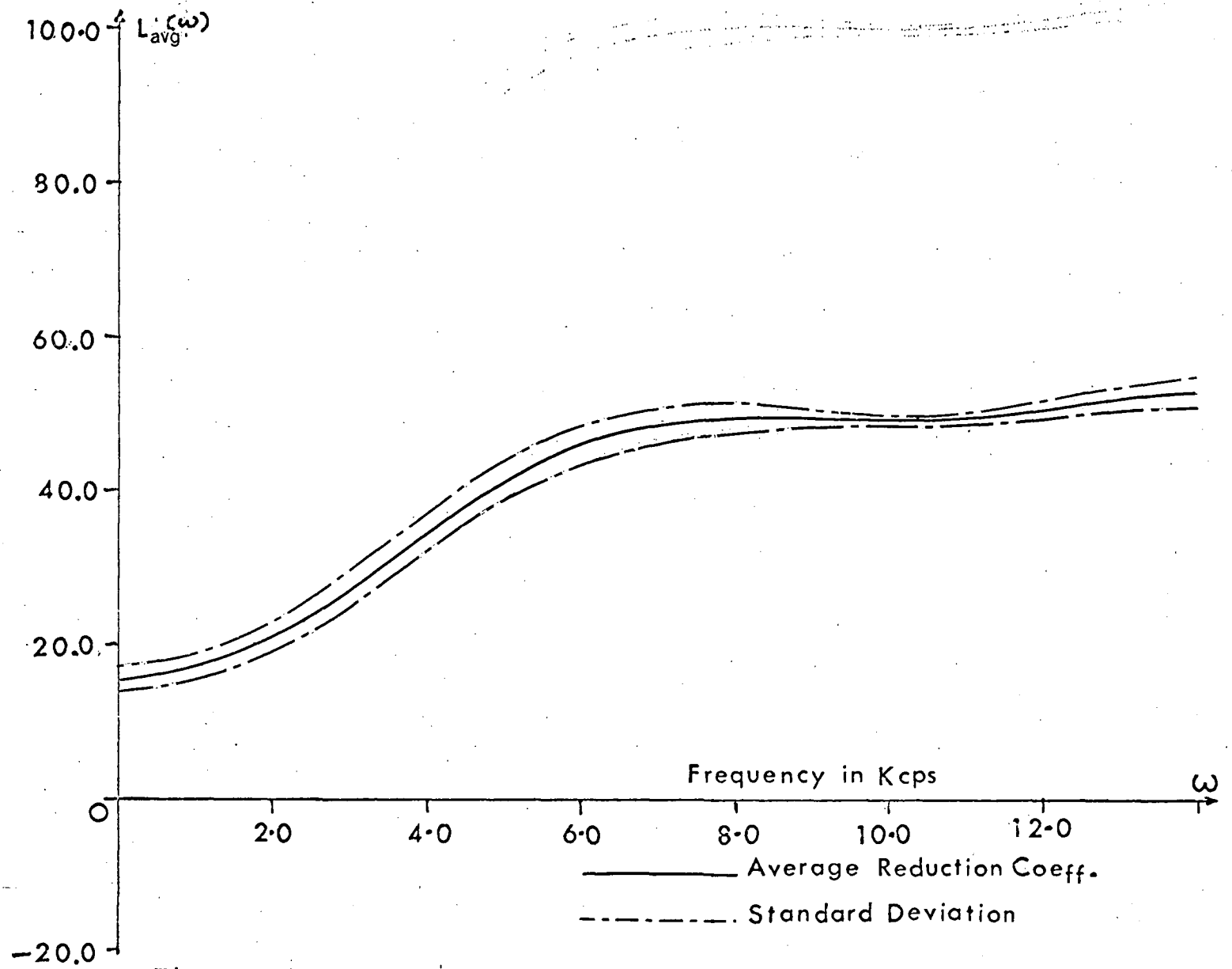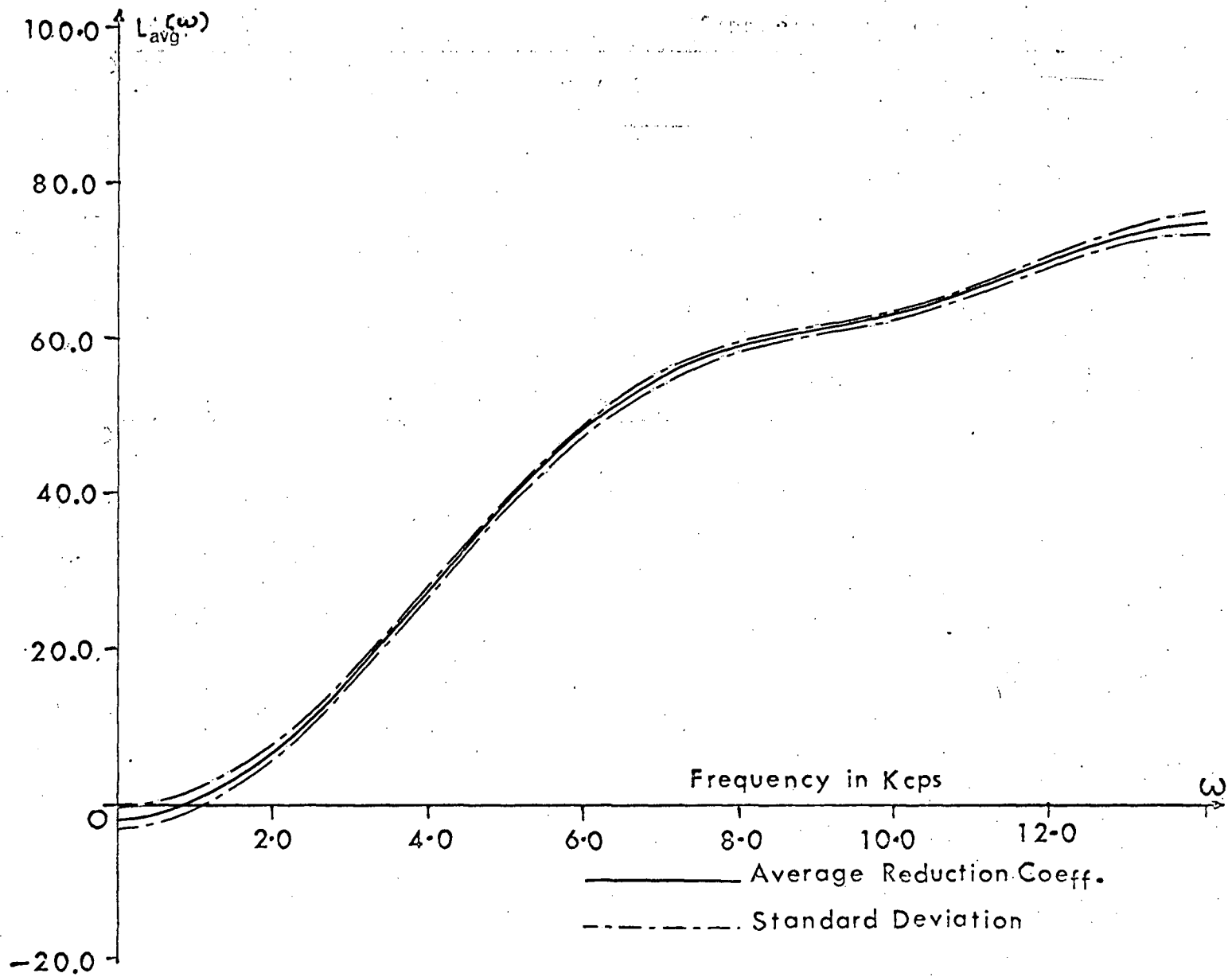Figure D.3 Average Reduction Coefficient for 0.75 in long 7% Antimonial Lead
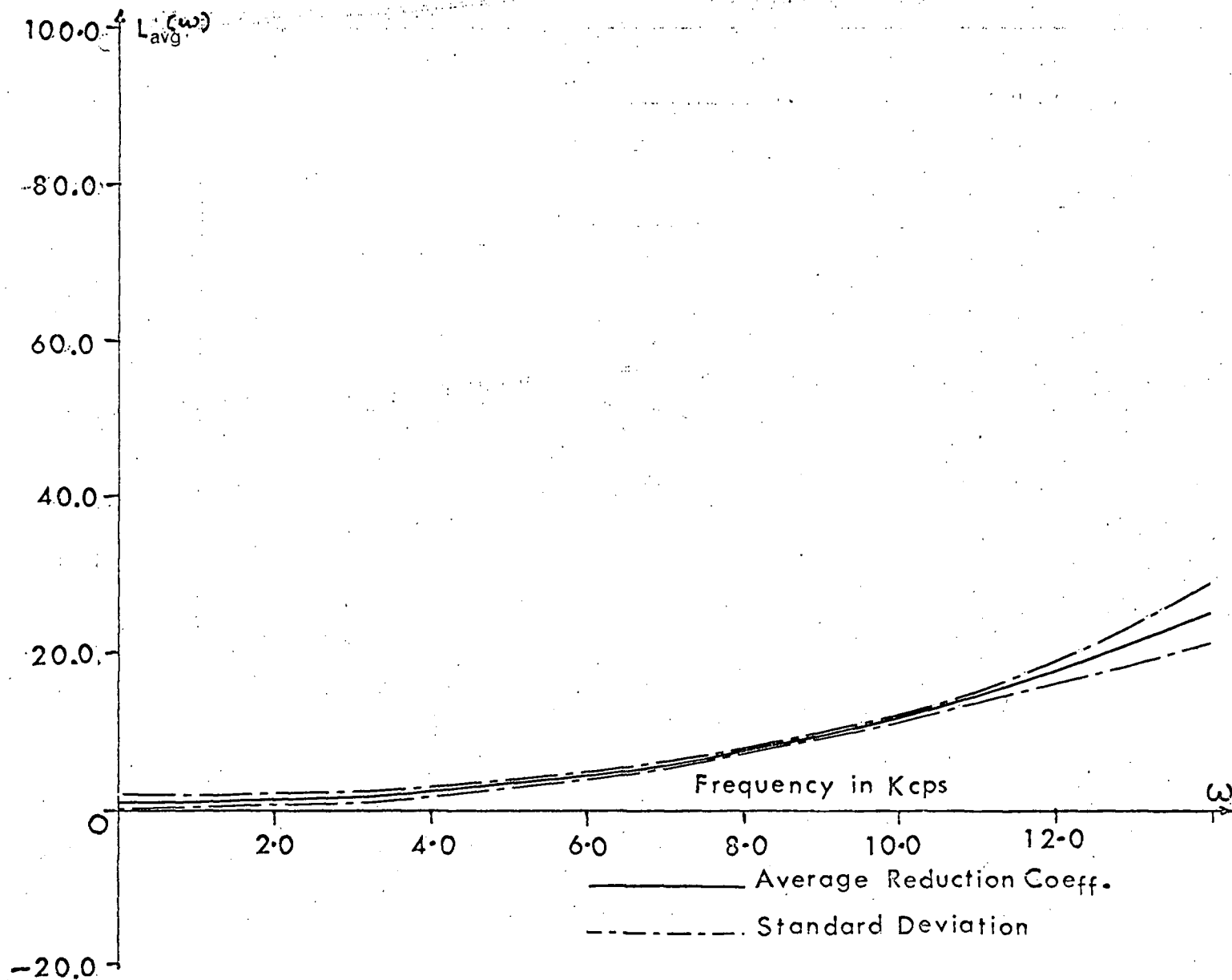
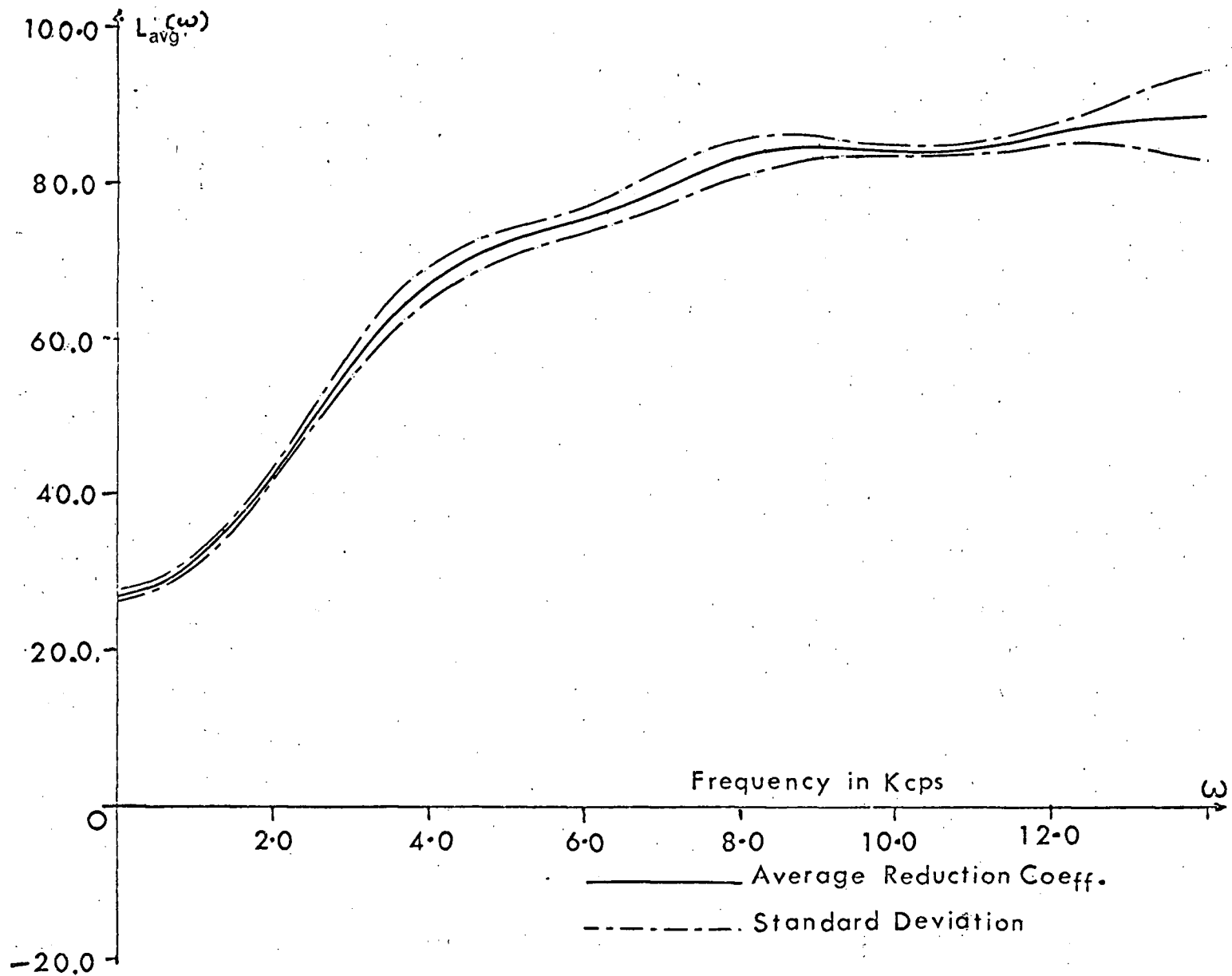Figure D.4   Average Reduction Coefficient for 0.25 in long 3%
Antimonial Lead
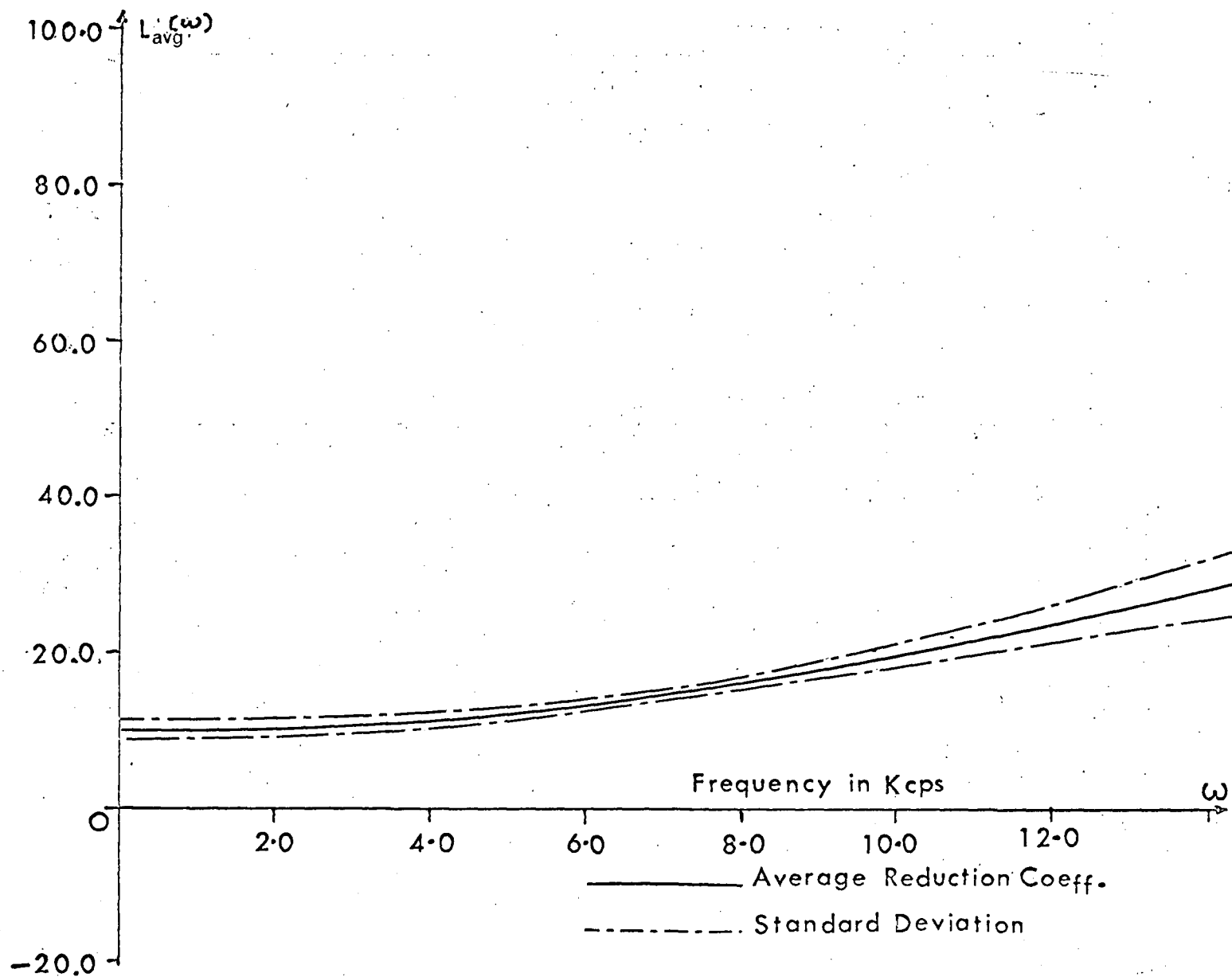
Figure D.5   Average Reduction Coefficient for 0.50 in long 3%
Antimonial Lead
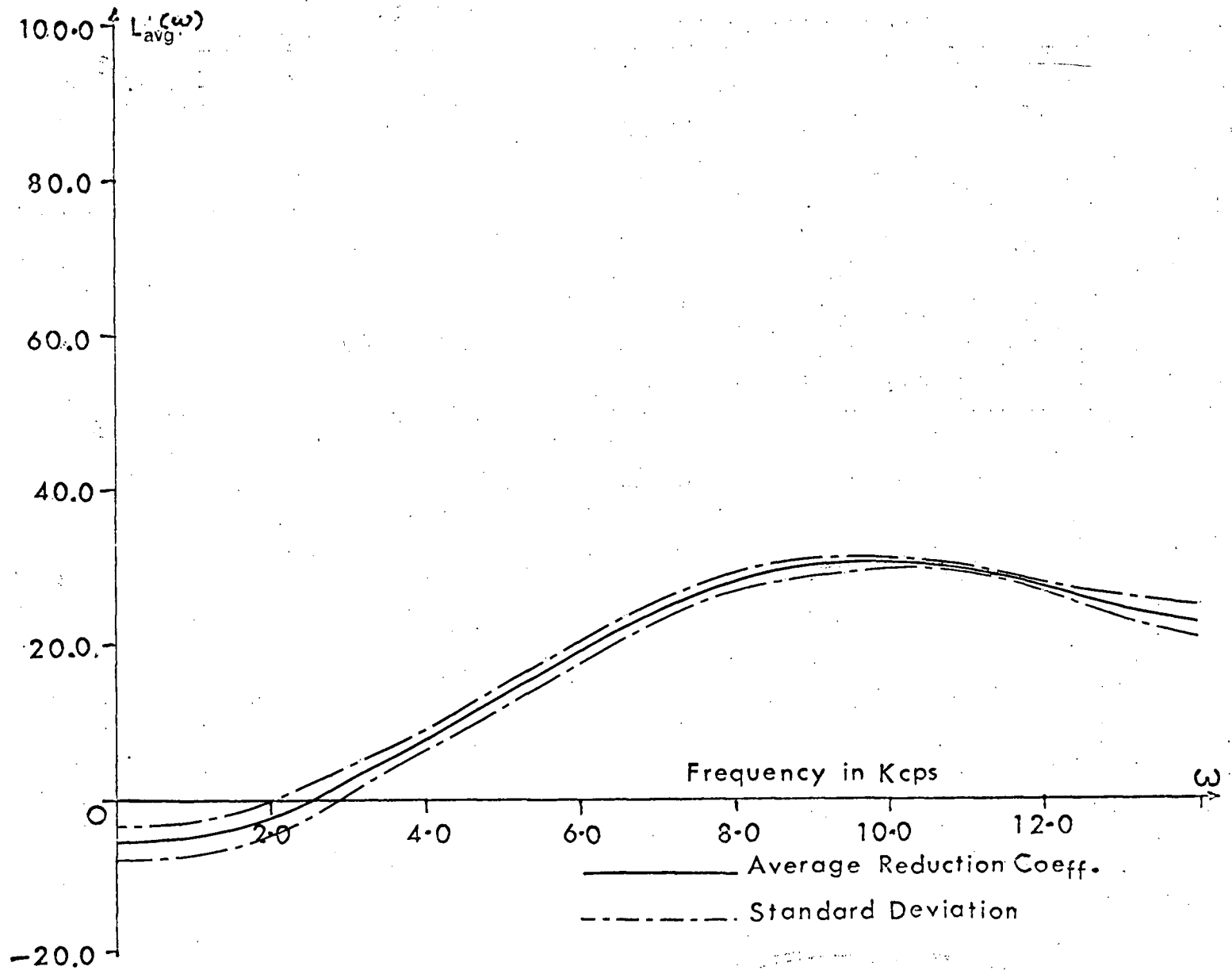
Figure D.6 Average Reduction Coefficient for 0.75 in long 3%
Antimonial Lead

Figure D.7   Average Reduction Coefficient for 0.25 in long Pure Lead

78

Figure D.8   Average Reduction Coefficient for 0.50 in long Pure Lead

Figure D.9 Average Reduction Coefficient for 0.75 in long Pure Lead

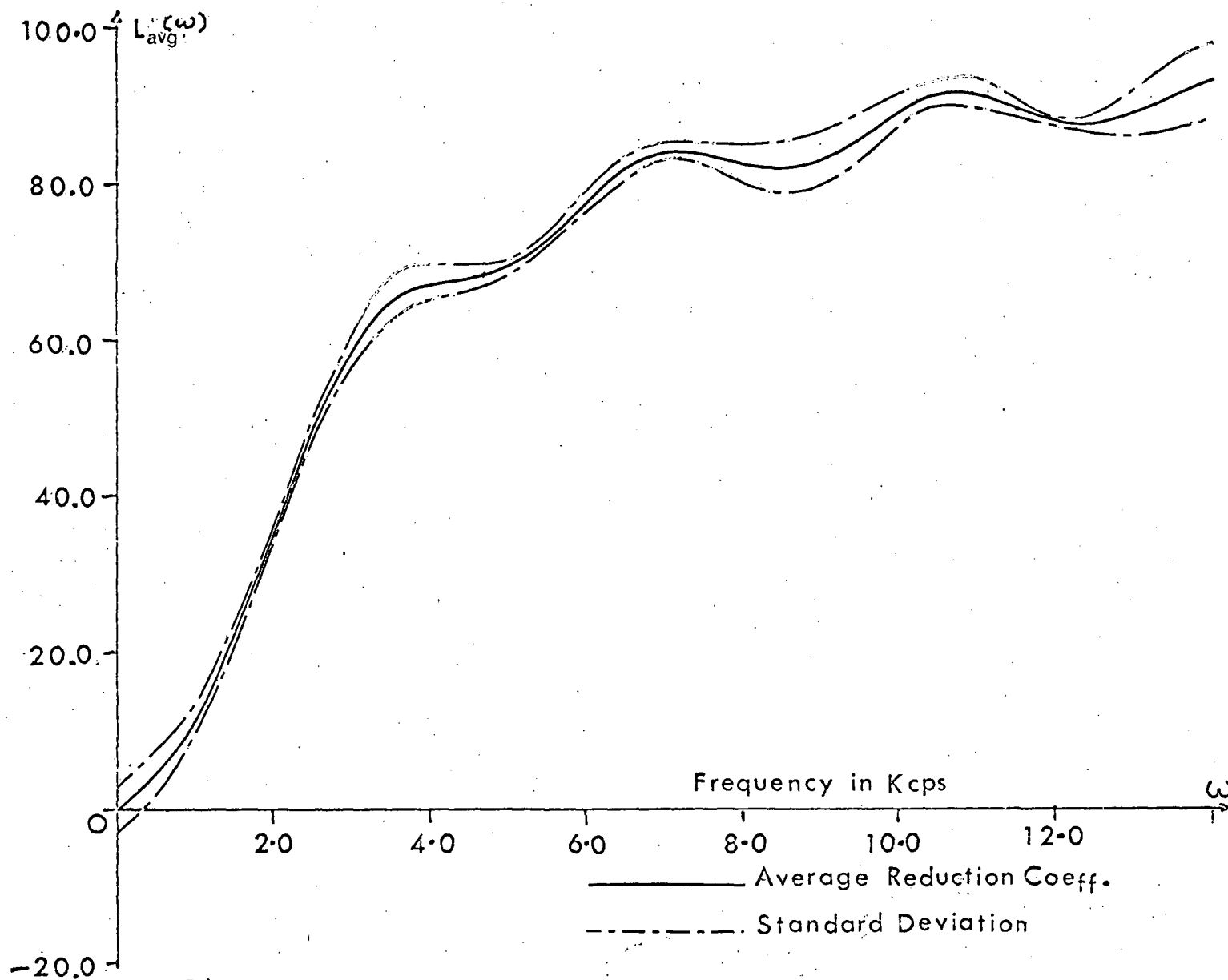Figure D.10   Average Reduction Coefficient for 0.25 in long Nylon

Fogire D.11   Average Reduction Coefficient for 0.50 in long Nylon

Figure D.12   Average Reduction Coefficient for 0.75 in long Nylon

ii) Transmission Coefficient:

If a stress wave travelling in an elastic bar is given by

$$u = f(t-\frac{x}{c}) = D(\omega) \sin\{\omega(t-\frac{x}{c}) + \psi\} \qquad (9.D.1)$$

Then stress can be expressed as

$$\sigma = -\frac{E}{c} f'(t-\frac{x}{c}) = -\frac{E}{c} D(\omega) \cos\{\omega(t-\frac{x}{c} + \psi\}$$

$$(9.D.2)$$

$$= G(\omega) \sin\{\omega(t-\frac{x}{c}) + \phi\}$$

The intensity of a wave can be expressed as the average energy over the period of the wave crossing per unit area per unit time. The expression for the energy, over a period T_0 of the wave, crossing per unit area at a distance x along the length, can be written as

$$E_n(\omega) = [\text{ Strain Energy + Kinetic Energy }]_{x/c}^{T_0+x/c}$$

$$(9.D.3)$$

$$= \frac{1}{2E}\int_{x/c}^{T_0+x/c} \sigma^2 c\,dt + \frac{1}{2}\rho \int_{x/c}^{T_0+x/c} \dot{u}^2 c\,dt$$

$$= \frac{c}{2E} \int_{x/c}^{T_o+x/c} \frac{E^2}{c^2} f'^2(t-\frac{x}{c})\, dt + \frac{1}{2}\rho c \int_{x/c}^{T_o+x/c} f'^2(t-\frac{x}{c})\, dt$$

$$(9.D.4)$$

$$= \frac{c}{E} \int_{x/c}^{T_o+\frac{x}{c}} \frac{E^2}{c^2} f'^2(t-\frac{x}{c})\, dt \qquad\qquad (9.D.5)$$

$$= \frac{c}{E} \int_{x/c}^{T_o+\frac{x}{c}} G^2(\omega)\, \sin^2\{\omega(t-\frac{x}{c}) + \phi\}\, dt \qquad (9.D.6)$$

$$= \frac{cT_o}{2E} G^2(\omega) \ . \qquad\qquad\qquad (9.D.7)$$

Therefore the intensity $I(\omega)$ can be expressed as

$$(9.D.8)$$

$$I(\omega) = \frac{c}{2E} G^2(\omega).$$

The transmission coefficient $\alpha_T(\omega)$ is given as the ratio of the intensities of the transmitted wave to the incident wave. Thus in present context of a three bar system

$$\alpha_T(\omega) = \frac{I^t(\omega)}{I^i(\omega)} = [\ \frac{G^t(\omega)}{G^i(\omega)}\ ]^2 = [\ 1-L(\omega)\ ]^2 \ . \qquad (9.D.9)$$

The following figures (Figures D.13 through D.16) show the variation of $\alpha_T(\omega)$ with frequency ω, which have been plotted corresponding to $L_{avg}(\omega)$ values shown in Figure D.1 through D.12.
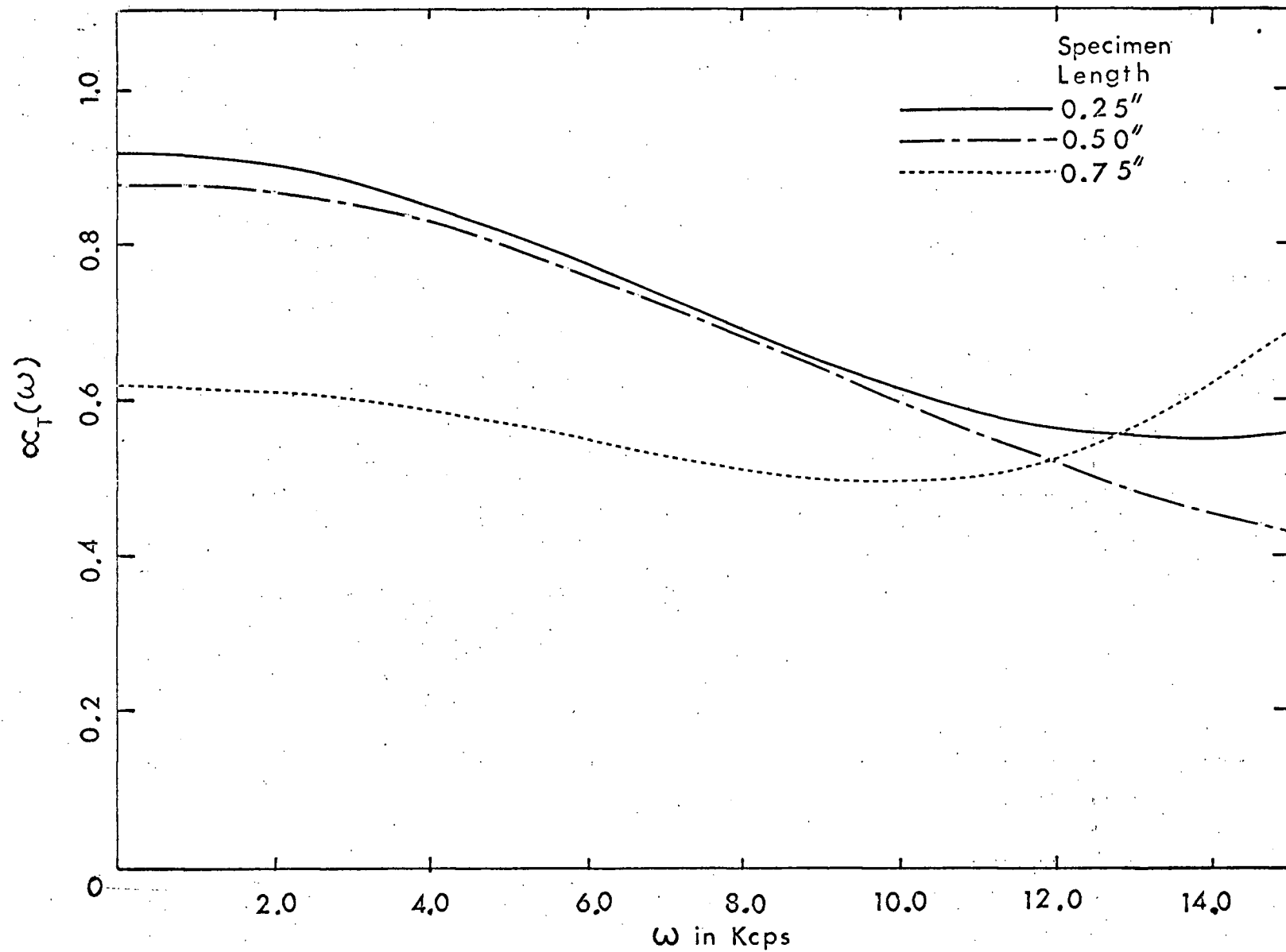
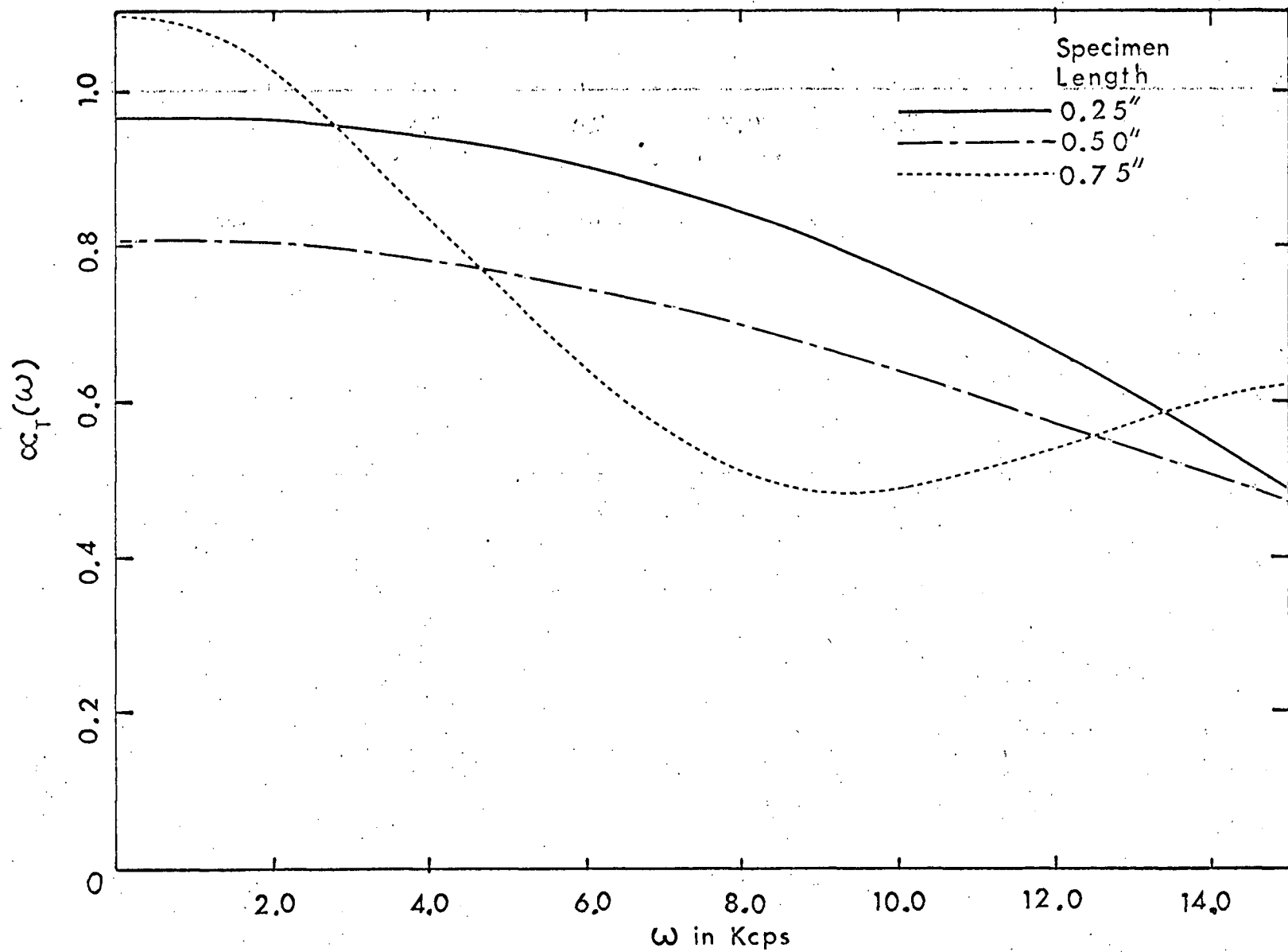Figure D.13   Transmission Coefficient for 7% Antimonial Lead

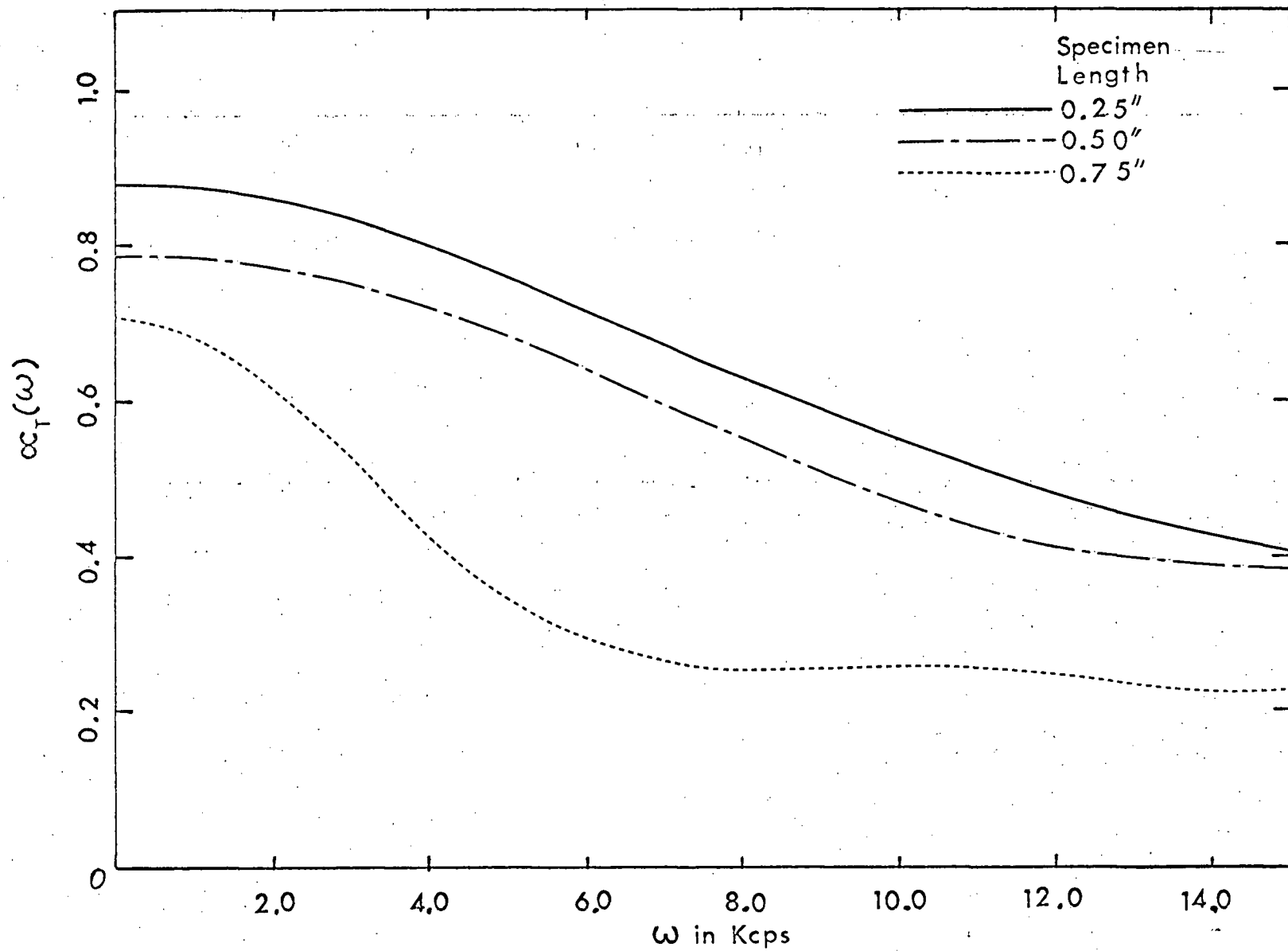Figure D.14   Transmission Coefficient for 3% Antimonial Lead

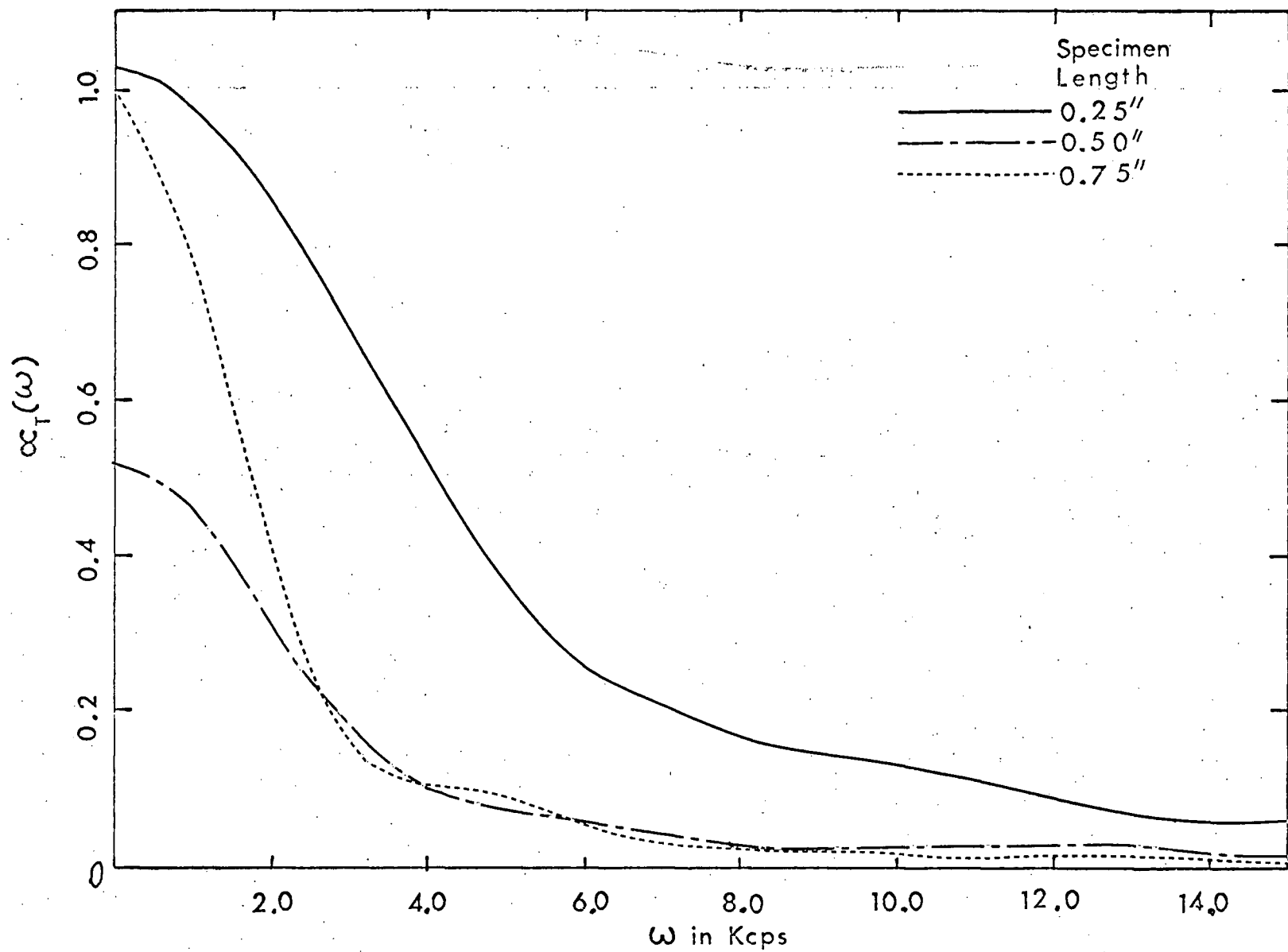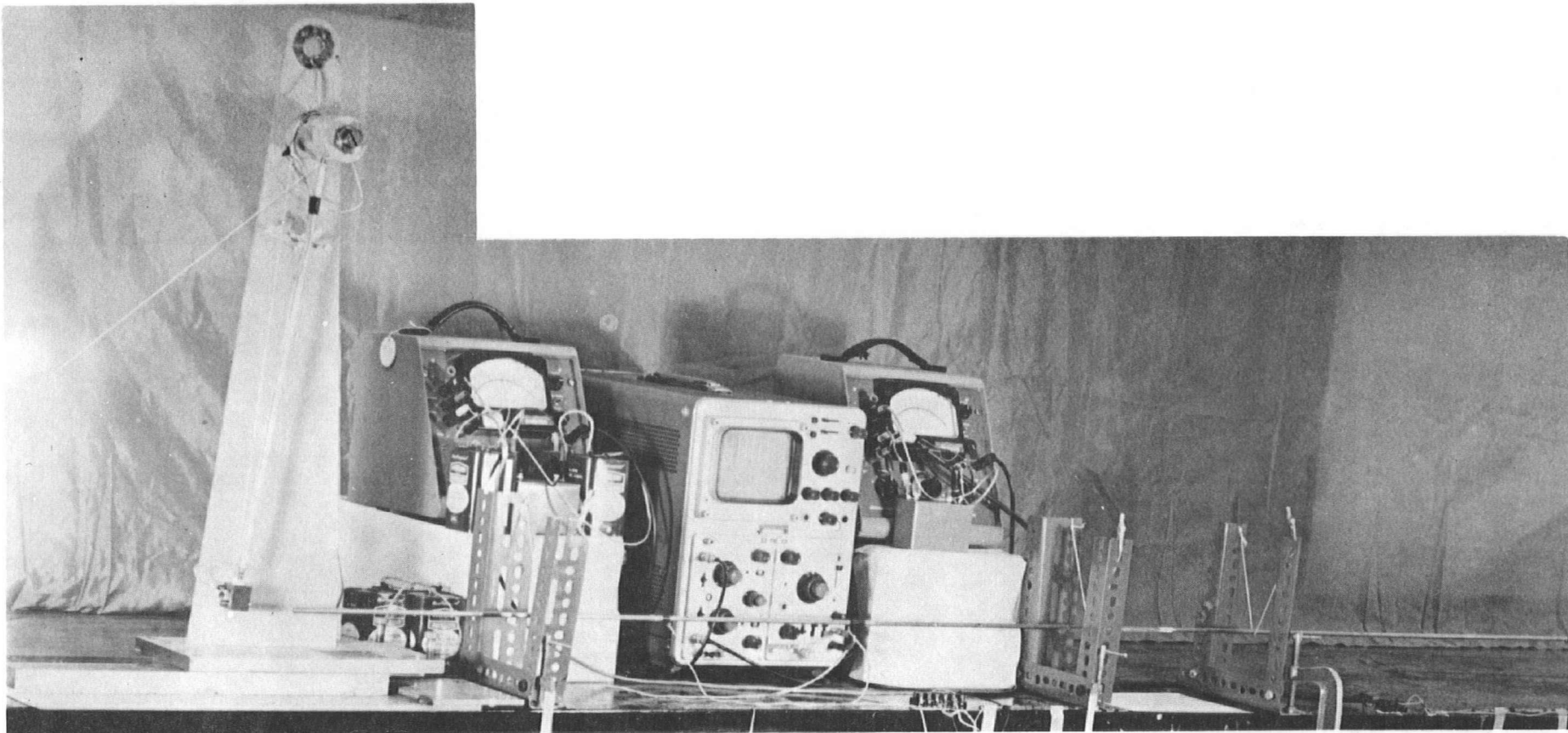Figure D.15 Transmission Coefficient For Pure Lead

Figure D.16   Transmission Coefficient For Nylon

Figure D.17   Experimental Setup